***Carnets Geol.* 26 (17)**

EISSN 16340744
DOI: 10.2110/carnets.2026.2617

Serra Gelada (Alicante, Spain): Evidence and implications of a paleo-island setting during the Jurassic-Cretaceous transition

Bruno R.C. GRANIER [1]
José Enrique TENT-MANCLÚS [2, 3, 4]
Jingyi YANG [5]
Emmanuel ROBERT [1, 6]
Antonio ESTÉVEZ RUBIO [3, 7]
Davide BONOMO [2, 8]

Abstract: This study revisits the uppermost Jurassic-lowermost Cretaceous succession of Serra Gelada (Alicante, SE Spain) based on new field observations and petrographic analyses. It is the second publication presenting and discussing results and interpretations of the PhD thesis of the first author, defended forty years ago. Several previous interpretations, including the identification of mud-mound facies, tectonic breccias, and hardgrounds, are reassessed.

The Tithonian-lower Berriasian limestones are reinterpreted as deposits formed in very shallow-marine environments, ranging from subtidal to intertidal settings and strongly influenced by microbial activity. A major outcome of this study is the recognition of a genuine paleokarst system comprising dolines, caves, chimneys, and chaotic collapse breccias. These features record a significant phase of subaerial exposure during the late Berriasian-early Valanginian and indicate that Serra Gelada formed a small paleo-island, most likely uplifted through salt tectonics involving Triassic evaporites. During the Valanginian transgression, wave erosion produced an abrasion surface across the karstified rocky substrate, while marine sediments progressively infilled the cavities and fractures, ranging from microscopic to decimetric scale. In addition to collapse breccias, coloured micritic infills help visualize repeated episodes of fracturing, cementation, and sediment percolation from the Valanginian to the earliest Aptian. These processes are interpreted in relation to the extensional tectonic phase that affected the External Zones of the Betic Range. Petrographic and cathodoluminescence analyses reveal a complex cement stratigraphy recording successive stages of early marine cementation, meteoric-phreatic diagenesis with limited marine mixing, and later burial diagenesis.

[1] *State Key Laboratory of Palaeobiology and Oil Stratigraphy, Nanjing Institute of Geology and Palaeontology, Chinese Academy of Sciences, Nanjing 210008 (China);*
Membre correspondant, Muséum d'Histoire Naturelle (MHN), Route de Malagnou 1, 1208 Genève (Switzerland);
2 impasse Charles Martel, F-29217 Plougonvelin (France)
brcgranier@free.fr

[2] *Instituto Multidisciplinar para el Estudio del Medio - IMEM "Ramón MARGALEF", Universidad de Alicante (Spain)*

[3] *Ciencias de la Tierra y del Medio Ambiente, Universidad de Alicante, Ap. de correos, 99, 03080 Alicante (Spain)*

[4] *je.tent@ua.es*

[5] *State Key Laboratory of Palaeobiology and Oil Stratigraphy, Nanjing Institute of Geology and Palaeontology, Chinese Academy of Sciences, Nanjing 210008 (China)*
jyyang@nigpas.ac.cn

[6] *Laboratoire de Géologie de Lyon, CNRS, Univ Lyon, UCBL, ENSL, UJM, LGL-TPE, F-69622, Villeurbanne (France)*
emmanuel.robert@cnrs.fr

[7] *antonio.estevez@ua.es*

[8] *davide.bonomo@ua.es*

Published online in final form (pdf) on September 14, 2026
[Editor: Jordi PÉREZ-CANO; Robert W. SCOTT; technical editor: Bruno R.C. GRANIER]

This revised interpretation provides a more robust reconstruction of the geological evolution of Serra Gelada and contributes to a better understanding of the paleogeographic evolution of the Prebetic domain during the Jurassic-Cretaceous transition.

Keywords:

- Benidorm;
- Prebetic domain;
- Jurassic-Cretaceous transition;
- carbonate sedimentology;
- diagenesis;
- paleo-island;
- paleokarst;
- salt tectonics

Citation: GRANIER B.R.C., TENT-MANCLÚS J.E., YANG Jingyi, ROBERT E., ESTÉVEZ RUBIO A. & BONOMO D. (2026).- Serra Gelada (Alicante, Spain): Evidence and implications of a paleo-island setting during the Jurassic-Cretaceous transition.- *Carnets Geol.*, Madrid, vol. 26, no. 17, p. 377-407. DOI: 10.2110/carnets.2026.2617

Résumé : ***Serra Gelada (Alicante, Espagne) : Indices de l'existence d'une île fossile à la transition Jurassique-Crétacé et ses implications.***- Cette étude présente une révision de la succession du Jurassique terminal-Crétacé basal de la Serra Gelada (Alicante, sud-est de l'Espagne) à partir de nouvelles observations de terrain et d'analyses pétrographiques. Il s'agit de la deuxième publication présentant et discutant les résultats et les interprétations issus de la thèse de doctorat du premier auteur, soutenue il y a quarante ans. Plusieurs interprétations antérieures, notamment l'identification de faciès de monticules de boue (*mud-mounds*), de brèches tectoniques et de fonds durcis (*hardgrounds*), sont réévaluées.

Les calcaires du Tithonien-Berriasien inférieur sont réinterprétés comme des dépôts formés dans des environnements marins très peu profonds, allant de milieux subtidaux à intertidaux et fortement influencés par l'activité microbienne. Un résultat majeur de cette étude est la reconnaissance d'un véritable système paléokarstique comprenant des dolines, des grottes, des cheminées et des brèches chaotiques d'effondrement. Ces structures témoignent d'une importante phase d'émersion au cours du Berriasien supérieur-Valanginien inférieur et indiquent que la Serra Gelada a temporairement formé une île, probablement à la suite d'un soulèvement localisé du substratum sous l'effet d'une tectonique salifère impliquant des évaporites triasiques. Lors de la transgression valanginienne, l'érosion par les vagues a produit une surface d'abrasion sur le substrat rocheux karstifié, tandis que des sédiments marins ont progressivement rempli les cavités et les fractures, dont les dimensions vont de l'échelle microscopique à l'échelle décimétrique. Outre les brèches d'effondrement, les remplissages micritiques colorés permettent de mettre en évidence des épisodes répétés de fracturation, de cimentation et de percolation sédimentaire, du Valanginien jusqu'à l'Aptien basal. Ces processus sont interprétés en relation avec la phase tectonique extensive qui a affecté les Zones externes de la chaîne Bétique. Les analyses pétrographiques et en cathodoluminescence révèlent une stratigraphie complexe des ciments, enregistrant des étapes successives de cimentation marine précoce, de diagenèse météorique-phréatique avec des épisodes rares et courts de mélange avec des eaux marines, puis de diagenèse d'enfouissement.

Cette réinterprétation permet une reconstitution plus robuste de l'évolution géologique de la Serra Gelada et contribue à une meilleure compréhension de l'évolution paléogéographique du domaine prébétique au cours de la transition Jurassique-Crétacé.

Mots-clefs :

- Benidorm ;
- domaine prébétique ;
- transition Jurassique-Crétacé ;
- sédimentologie des carbonates ;
- diagenèse ;
- île fossile ;
- paléokarst ;
- tectonique salifère

1. Introduction

Since the work of VERNEUIL and COLLOMB (1853: p. 93), Serra Gelada (Fig. 1.A) has been recognized as one of the four emblematic localities of the Prebetic of Alicante where shallow-water uppermost Jurassic-lowermost Cretaceous strata are exposed (Fig. 1.D). It lies only a few kilometers south of the Altea diapir, the largest diapir in the eastern Betic Range (RÍOS GARCÍA *et al.*, 1960; NAVARRO *et al.*, 1962). The occurrence of Jurassic strata at Serra Gelada was first recognized in the doctoral thesis of the first author (GRANIER, 1987), although these strata had previously been assigned to the Neocomian (*e.g.*, RÍOS GARCÍA *et al.*, 1960; see GRANIER, 1987: Fig. 20 and references therein). However, this pioneering work contained several shortcomings and inaccuracies that became apparent only later, particularly in light of subsequent advances in systematic paleontology, carbonate sedimentology, and holostratigraphy.

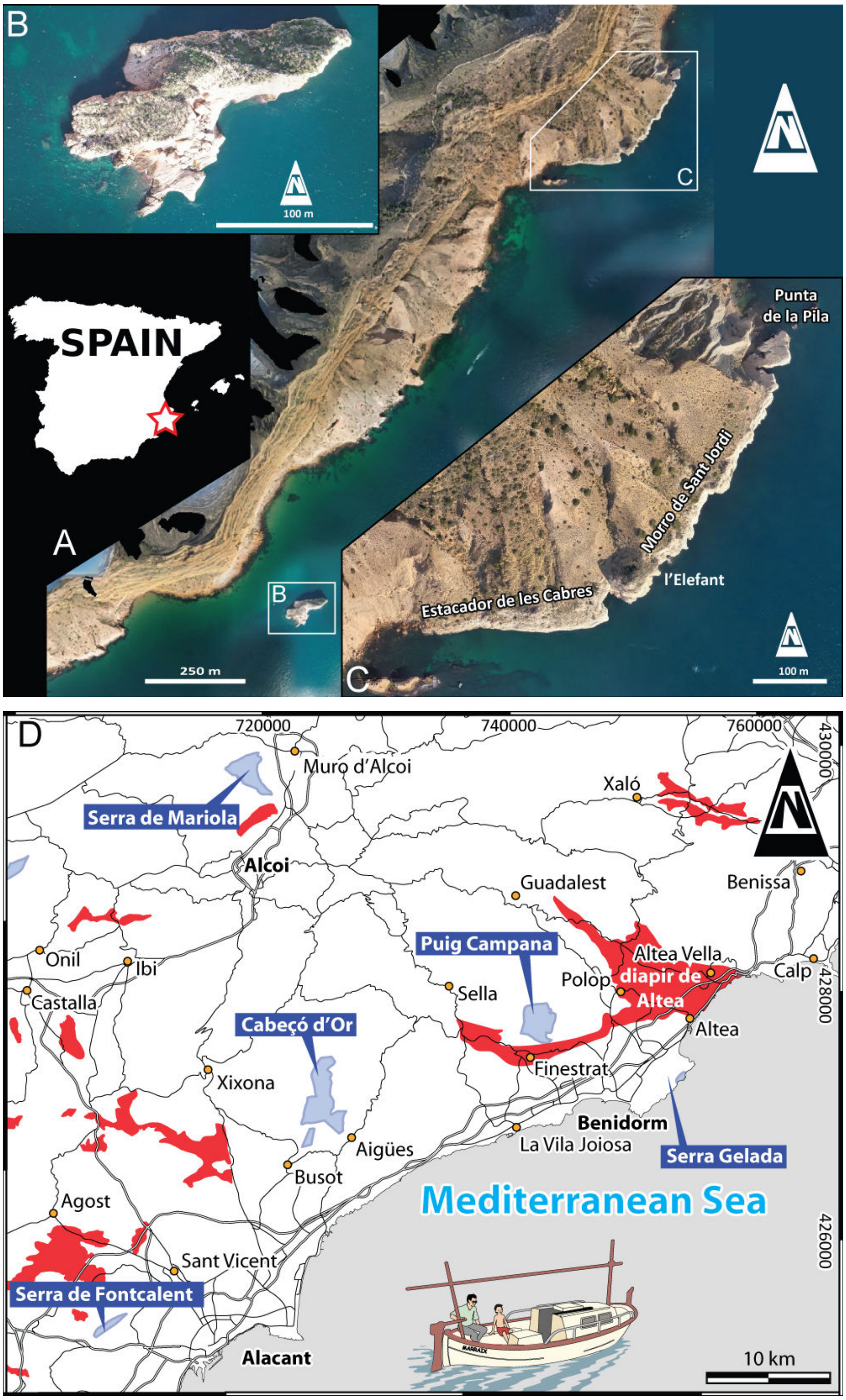

◀ **Figure 1: A-C:** Drone photographs of the Serra Gelada area on the coast of Alicante Province (SE Spain); A: orthophoto of the marine sector of Serra Gelada, produced by processing approximately 9,000 photographs acquired during drone surveys carried out in 2025; **B:** close-up view of Isleta Mitjana; **C:** close-up view of the Morro de Sant Jordi sea cliff; **D:** location map of Triassic salts (in red), including the Altea diapir, and five areas with Upper Jurassic outcrops (four with shallow-water facies: Cabeçó d'Or, Puig Campana, Serra de Mariola, and Serra Gelada; one with deeper-water facies: Serra de Fontcalent). The Marraix boat icon at the bottom of the figure was redrawn from Jaume Fuster and Joan Fuster (2017).

The present study therefore constitutes the second publication to revisit and discuss the results and interpretations derived from this PhD thesis, following the first revision of the Aptian-Albian interval presented by Granier *et al.* (2025).

Here, we focus on the lowermost part of Serra Gelada succession, below the Aptian marls, reassessing previous observations and interpretations in light of new field and petrographic evidence, and discuss the implications of these findings. Particular attention is paid to the uppermost Jurassic-lowermost Cretaceous transition, which preserves a diverse assemblage of unusual sedimentary and diagenetic features, the origin and significance of which have until now remained poorly understood.

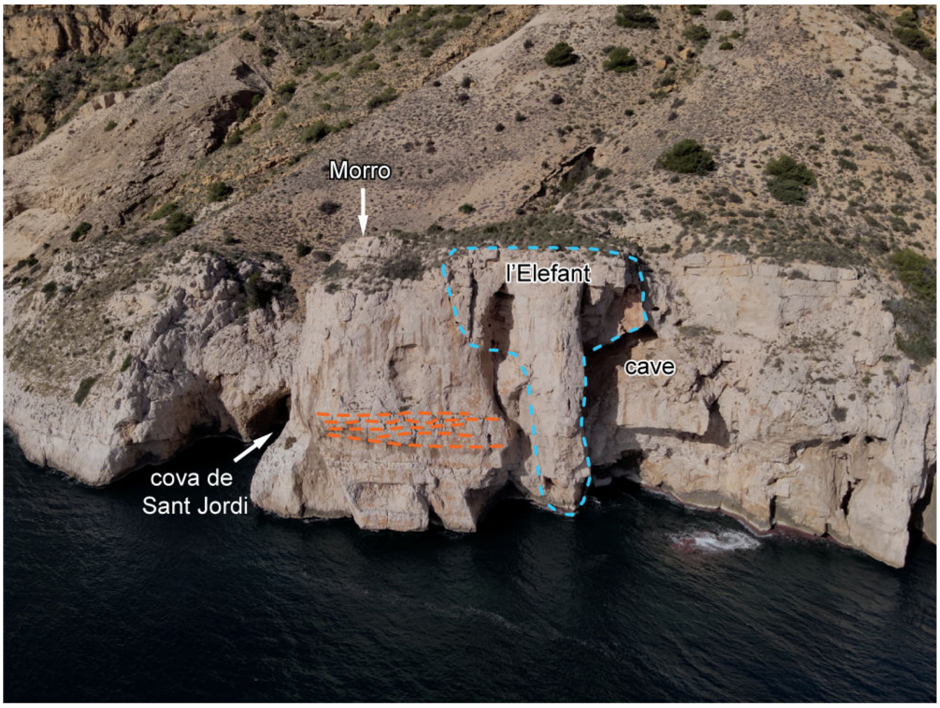

◀ **Figure 2:** "L'Elefant" is a portion of the Morro de Sant Jordi sea cliff that, when seen from the sea, resembles an elephant face, the two ears and the trunk. The left side of the "elephant" is defined by a fracture, whereas the right ear, the eastern one, is made by a paleocave, here referred to as the l'Elefant Cave. The "Morro" marks the highest point of the sea cliff at the promontory. The "cova de Sant Jordi" indicates a small cave containing a black stain on its inner wall that, when viewed from the sea, resembles the figure of Sant Jordi (Saint George). Sigmoidal bedding (orange dotted lines) exposed to the left of the l'Elefant is also highlighted. Photograph acquired using a drone.

The main questions examined in this study are therefore: 1) what depositional environments are represented by the Tithonian-lower Berriasian limestones at Serra Gelada; 2) what processes produced the cavities, breccias, substratiform fractures, and coloured micritic geopetal infills; 3) when did these processes take place; and 4) what were the respective roles and timing of eustatic sea-level changes and regional versus local tectonics in producing local emergence and subsequent submergence? Answering these questions is essential for establishing the geological history of this locality and assessing its significance within the broader paleogeographic evolution of the Prebetic domain.

To address these questions, we combine a review of previous data (*e.g.*, GRANIER, 1987) with new field observations at Morro de Sant Jordi and Isleta Mitjana, together with petrographic, scanning electron microscopy, and cathodoluminescence analyses. Particular attention is paid to the morphology of the upper surface of the Jurassic limestones, the geometry and infilling of cavities and fractures, the nature of the breccias, and the diagenetic sequence recorded by the cement stratigraphy. These observations are integrated with the biostratigraphic and sedimentological framework established at nearby localities, particularly Puig Campana and Cabeçó d'Or.

The primary aim is to reassess the nature and significance of the stratigraphic hiatus at the Jurassic/Cretaceous boundary at Serra Gelada. More broadly, this study seeks to clarify the paleogeographic and tectono-sedimentary significance of this record for the Prebetic domain during the Jurassic-Cretaceous transition, including the possible role of Triassic evaporites in generating localized positive relief. This integrated reinterpretation also provides a framework for distinguishing primary depositional surfaces from subsequent erosional and diagenetic features, including hardgrounds, rocky substrates, karst surfaces, and cement-related fabrics.

2. General setting

As initially reported by the first author (GRANIER, 1987), uppermost Jurassic strata are exposed only at the base of the Serra Gelada sea cliff, at two spots (Fig. 1.A): 1) the Morro de Sant Jordi promontory, altitude ~ 40 m (Fig. 1.C), and 2) Isleta Mitjana or Penyes d'Arabi, altitude 29 m (Fig. 1.B).

1) Although Morro de Sant Jordi can be accessed by land (Alfonso YÉBENES, personal communication), the route is relatively hazardous. Consequently, as on previous occasions (1984-1985 and 2010), we reached this spot of interest by sea. During his PhD studies, the first author (BRCG) visited the locality only twice (on 25/07/1984 and 28/10/1985). At that time, his field work focused primarily on sampling the Jurassic limestones and the overlying condensed section with ferruginous oncoids, as well as collecting Cretaceous ammonites for biostratigraphic purposes. Twenty-five years later (on 22/09/2010), he returned to the site with the late Bernard CLAVEL, the late Robert BUSNARDO, and colleagues from the University of Alicante, including the fifth author (AER), for a brief visit.

More recently, our team, led by the second author (JETM), obtained permission from the authorities of the Parc Natural de la Serra Gelada to conduct new geological investigations within the park, including at Morro de Sant Jordi. In the present paper, we present the results of the latest field campaign (15-16/06/2026), attended by three of us (BRCG, JETM, and DB).

2) Access to Isleta Mitjana is restricted because it is an important nesting site for seabirds and, consequently, a highly protected area within the park. On 22/11/2025, aboard the Marraix, skippered by Jaume FUSTER, we circumnavigated the islet without landing. On a separate occasion, however, the sixth author (DB) was able to land and collect a small number of rock samples that will be used to date the strata.

At the nearby Puig Campana, the uppermost Jurassic - lowermost Cretaceous sedimentary succession (GRANIER, 1987, 2019) comprises, from base to top (Table 1): 1) upper Tithonian - lower Berriasian limestones with *Aloisalthella* (formerly known as *Clypeina*, see GRANIER & LETHIERS, 2019); 2) middle Berriasian calcarenites and oolites with *Ichnusella* (formerly known as "*Neotrocholina*", see RIGAUD *et al.*, 2018); 3) upper Berriasian marls with *Falsolikanella*; 4) upper Berriasian limestones with *Coscinoconus* (formerly known as "*Trocholina*", see RIGAUD *et al.*, 2013); 5) lower Valanginian calcarenites with *Pseudocyclammina*; and 6) a condensed interval overlain by 7) Aptian ammonites marls.

In contrast, at Serra Gelada, according to GRANIER (1987), the succession comprises only the first, sixth, and seventh units, with units 2 to 5 considered absent.

Because it is not possible to distinguish the lower Berriasian strata from the Tithonian strata on biostratigraphic grounds (GRANIER, 2019), they are collectively referred to hereafter as the Jurassic limestones for the sake of simplicity.

The new investigations provide an opportunity to revise several previous interpretations and to correct a number of significant misconceptions, including the following:

- the lenticular morphologies within the Jurassic limestones with *Aloisalthella sulcata* (formerly known as *Clypeina jurassica*) at Morro de Sant Jordi were originally interpreted as mud mound facies (GRANIER, 1987: p. 93 *et seq.*; CASTRO JIMÉNEZ, 1998, p. 274);
- the so-called "olistolithe" (GRANIER, 1987: Pl. 13, fig. d) at the top of these Jurassic limestones was interpreted as having undergone lateral sliding;
- the upper surface of these limestones was interpreted as a hardground (GRANIER, 1987; YÉBENES, 1996; CASTRO JIMÉNEZ, 1998) on the basis of the occurrence of borings (YÉBENES, 1996; CASTRO JIMÉNEZ, 1998, p. 276);
- Isleta Mitjana was also interpreted as consisting of the same Jurassic limestones with *Aloisalthella sulcata* (GRANIER, 1987) as those exposed at Morro de Sant Jordi;
- the coloured (pale orange, pink, and red) micritic sedimentary infills of substratiform fractures were partly interpreted as "couches filons" (*i.e.*, sedimentary sills) emplaced during multiple fracturing episodes related to the extensional tectonic phase that affected both the Prebetic and Subbetic zones during the late Valanginian and post-Valanginian times (GRANIER, 1987). The same interpretation was extended to the associated breccias containing angular intraclasts and coloured micritic sedimentary infills;
- some small extraclasts forming the nuclei of ferruginous oncoids (GRANIER, 1987: Pl. 17, figs. c-d) were originally considered to have been derived from the lower Valanginian calcarenites with *Pseudocyclammina* (Unit 5).

Table 1: Formal and informal lithostratigraphic units in the studied area (arranged from base to top). Caption: a) Morro de Sant Jordi; b) Isleta Mitjana; c) Puig Campana; d) Cabeçó d'Or; e) Serra de Mariola; 1) and 2) discrete members (lower and upper, respectively).

units	modern names	former names	lithostratigraphic units	biostratigraphy	biozones	(a)	(b)	(c)	(d)	(e)
Unit 1	*Aloisalthella* limestones	*Clypeina* limestones	Fm Sierra del Pozo	upper Tithonian - lower Berriasian	*Aloisalthella sulcata* biozone	x	x	x	x	x
Unit 2	*Ichnusella* calcarenites and oolites	*Neotrocholina* calcarenites and oolites	Fm Serra de Mariola	middle Berriasian	"*Macroporella*" *embergeri* biozone		x	x	x	x
Unit 3	*Falsolikanella* marls	*Falsolikanella* marls	Fm Puig Campana (1)	upper Berriasian	*Falsolikanella campanensis* biozone			x	x	x
Unit 4	*Coscinoconus* limestones	*Trocholina* limestones	Fm Puig Campana (2)	(as above)	(as above)			x	x	x
Unit 5	*Pseudocyclammina* calcarenites	*Pseudocyclammina* calcarenites	Fm Cabeçó d'Or	lower Valanginian	*Pseudocyclammina lituus* biozone			x	x	x
Unit 6	ammonite marls (1)	condensed interval	Fm Serra Gelada (1)	Valanginian-Barremian		x	x	x	x	x
Unit 7	ammonite marls (2)	Aptian ammonites marls	Fm Serra Gelada (2)	uppermost Barremian-Aptian		x	x	x	x	x

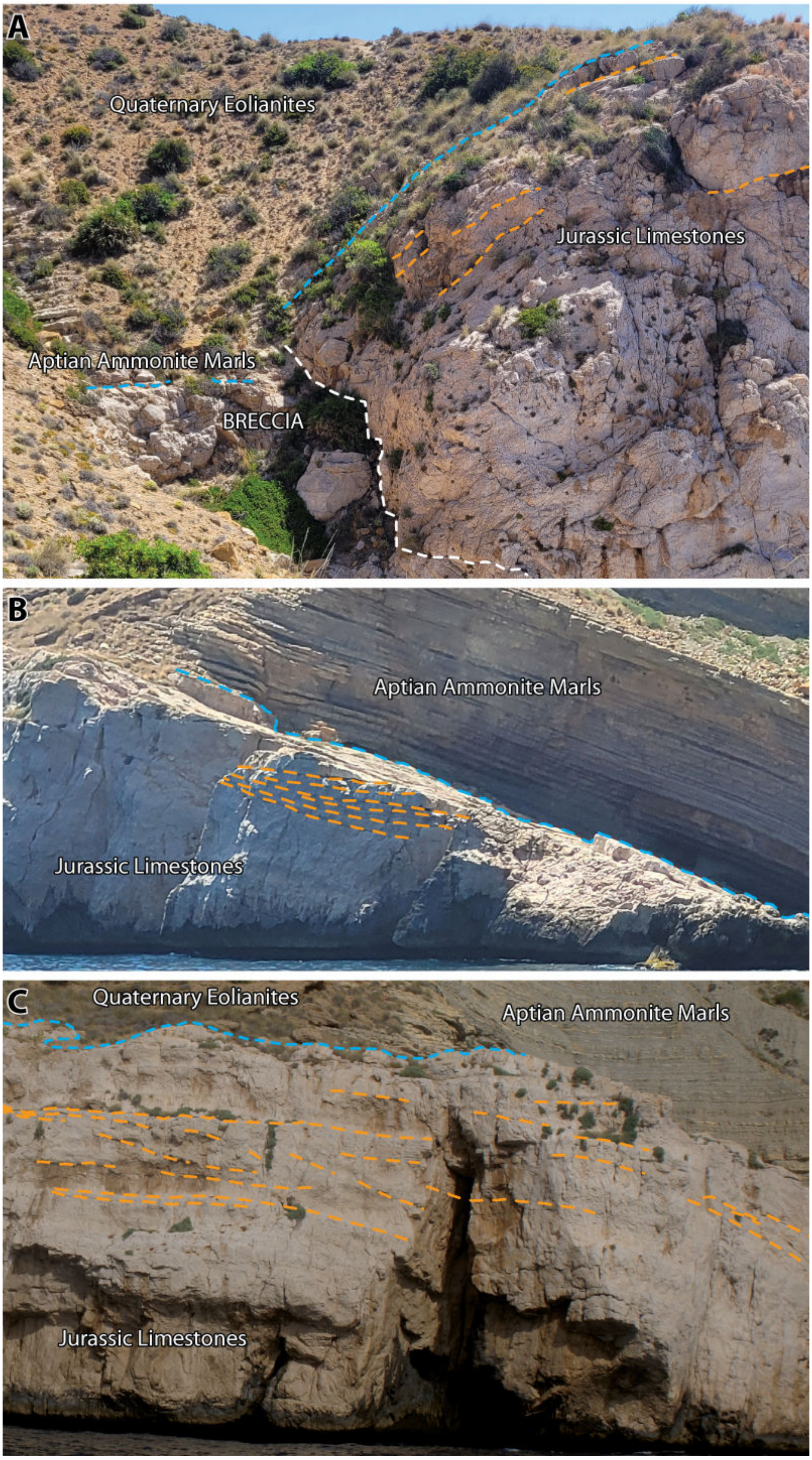

◀ **Figure 3: a:** View of the western side of l'Elefant (to be compared with GRANIER, 1987: Pl. 13, fig. b), showing Aptian ammonite-bearing marls draping a strongly contrasted Jurassic paleomorphology. Below the discontinuity (blue dotted line), the elevated area on the right corresponds to intact Jurassic limestones, whereas the lower area on the left side of the photograph corresponds to collapse breccias, which are characteristic of a doline. The boundary between the intact Jurassic limestones and the collapse breccias is marked by a white dashed line. **b-c:** Sigmoidal bedding (orange dotted lines) on the sea cliff near Punta de la Pila.

3. Material and methods

The total set of petrographic thin sections studied initially consisted of 59 thin sections prepared from 21 samples for Morro de Sant Jordi and 9 thin sections prepared from 4 samples for Isleta Mitjana. All these thin sections, together with three additional thin sections recently prepared in China (NIGPCAS) from samples SHJ 3bis and SHJ 19, are now registered in the collections of the 'Musée d'Histoire naturelle de Genève' under the numbers MHNG-GEPI-2024-11200 to 11224. Photomicrographs of the petrographic thin sections were taken using a digital MU900 AmScope camera mounted on a Leitz Diaplan microscope and a Wild/Heerbrugg M8 microscope. Additional thin sections and polished rock slabs were also prepared and are currently stored at the Departamento de Ciencias de la Tierra y del Medio Ambiente de la Universidad de Alicante.

Additional petrographic investigations were carried out by the first author (BRCG) during a two-month research stay (March-April 2026) at NIGPCAS (Nanjing, China) on small slabs prepared from samples SHJ 3bis and 19. These investigations included scanning electron microscopy (SEM) using a Hitachi SU3500 microscope and cathodoluminescence microscopy using a CITL Cathodoluminescence Mk5-2 system mounted on a Nikon Eclipse LV100N POL microscope.

Rather than using uncovered petrographic thin sections, the first author (BRCG) examined ultra-polished slabs, which provide a simpler, faster, and more cost-effective method for preparing rock samples for these cathodoluminescence analyses. However, it is worth noting that the distance between the upper surface of the slab and its ideal position in the vacuum chamber, as well as interference from light passing through the lead-glass viewing window in the microscope room, may affect the luminescence.

The same slabs were also used for SEM observations. Prior to SEM analysis, the slabs were briefly etched with 10% HCl. Areas previously exposed to the electron beam were found to be more resistant to acid etching; therefore, the slabs required additional polishing before the acid treatment to ensure uniform etching.

4. Previous observations and interpretations

4.1. Sedimentology

At Morro de Sant Jordi, specifically westward to cova de Sant Jordi and l'Elefant (Fig. 2), GRANIER (1987: Pl. 13, fig. b; here Fig. 3.a) described "bluish" Aptian "marls and argillaceous limestones that conform to the contrasting mound-and-furrow topography" of the white upper Tithonian-lower Berriasian limestones with *Aloisalthella* [translated from the French: "des marnes et calcaires argileux bleutés qui épousent des morphologies contrastées : monticules et sillons"].

The microfacies of these Jurassic limestones with *Aloisalthella* display a wide variety of microbial structures, ranging in thickness from a few tenths of a millimeter (*Gakhumella huberi* ZANINETTI, 1978, see GRANIER, 1987: Pl. 14, figs. e-f; Pl. 15, figs. a-c, f; Pl. 16, figs. g-i), to a few millimeters (micritic stromatolites resembling puffs of pipe smoke, see GRANIER, 1987: Pl. 15, figs. e, g; endostromatolites, see GRANIER, 1987: Pl. 15, fig. d; Pl. 16, figs. c-d; Pl. 17, figs. a-b; Pl. 51, figs. h-i; 2020: Figs. 3.B, 5.A-I; *Cayeuxia*-like structures, Pl. 1, fig. e *pars*, k-q; see GRANIER, 1987: Pl. 49, fig. i), to a few centimeters (*Bacinella*-like structures), with some structures extending laterally over several decimeters (micritized surfaces or microbial films, see GRANIER, 1987: Pl. 15, figs. h-i; 2020: Fig. 3.A). Peloids, including pelletoids, locally in fenestral facies (Pl. 2, figs. a-c), and coprolites (Pl. 2, fig. g), and (microbial) oncoids are the dominant allochems, with bioclasts occurring as subordinate constituents.

However, the contrasting topography and the microbial facies are not, by themselves, diagnostic of mud mounds, as erroneously inferred by GRANIER (1987), since both may develop independently in a variety of depositional environments. A revised interpretation of these features is presented later in the text, based on new field observations and petrographic evidence.

At Morro de Sant Jordi, more specifically at Punta de la Pila (Fig. 1.C), YÉBENES (1996) mentions "cavidades kársticas". In turn, CASTRO JIMÉNEZ (1998: p. 274) described a two-meter-deep "bolsada" located one meter below the top of the Jurassic limestones, whereas our most recent measurements (without taking the diverticula into account) indicate that it is approximately 2.2 m high and 2.5 m wide and that, at its uppermost point, lies approximately 2.3 m below the unconformity surface. Angular clasts, ammonites, and belemnites are among the allochems observed in its complex sedimentary infill. This first cave, which was not identified by GRANIER, is herein referred to as the YÉBENES paleocave (Pl. 3, figs. a-c). Moreover, GRANIER (1987) had also overlooked early leaching features, which, although uncommon, are preserved in some of the thin sections examined in the original material. Their significance is reassessed in the light of new observations, and a revised interpretation is presented later in the text.

Still at Punta de la Pila (Fig. 1.C), the so-called "olistolithe" (GRANIER, 1987: Pl. 13, fig. d; here Pl. 3, figs. a-b with an orange arrow, Pl. 4, figs. b-c) at the top of the Jurassic limestones is merely the expression of step-like relief, according to CASTRO JIMÉNEZ (1998: p. 275, Fig. 3.12.2b). Contrary to the interpretation of GRANIER (1987), the joint at the base of the block is not a glide plane. CASTRO JIMÉNEZ (1998) estimated the height of the step to be 1.3 m, whereas our most recent measurements indicate that it reaches up to 1.7 m. Near the step edge, two smaller, partly infilled depressions are draped by the bluish Aptian marls and argillaceous limestones. CASTRO JIMÉNEZ (1998) interpreted them as kamenitzas.

Laterally, the upper surface of the Jurassic limestones displays clavate borings (*e.g.*, *Gastrochaenolites*) beneath the condensed layer containing ferruginous oncoids (Pl. 4, fig. h). Although this surface is planar, it cuts across the underlying bedding at a slight angle. It strikes N45°E and dips 25° toward the NW, whereas the underlying bedding plane strikes N35°E and dips 15° toward the NW. The smallest angle between

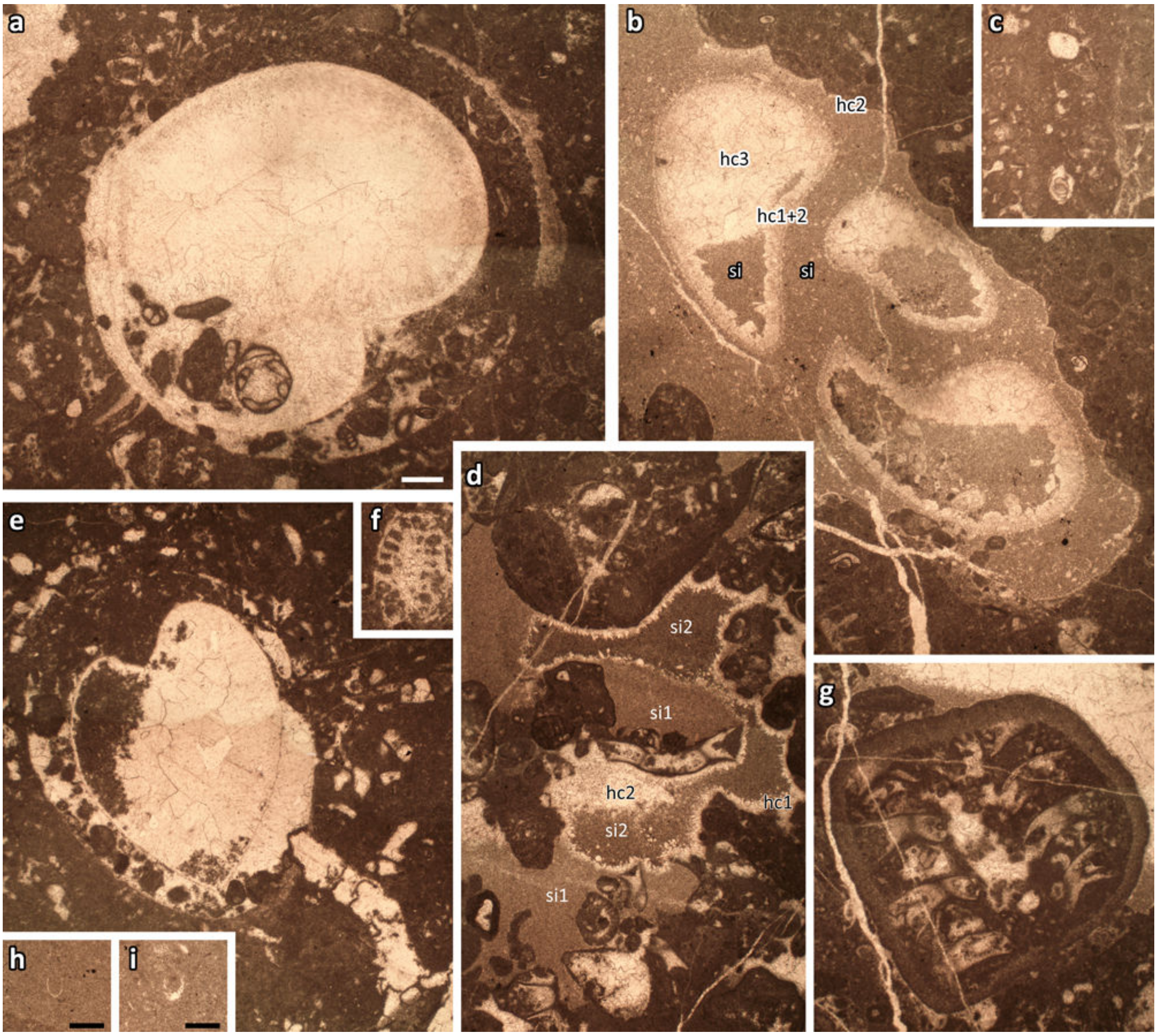

Figure 4: Morro de Sant Jordi. **a:** pholadid boring in a wackestone intraclast; **b:** diagenetic sequence with micritisation of the gastropod shell, cement 1 (hc1) in intragranular pores, leaching of the gastropod shell in the meteoric vadose zone, cement 2 (hc2), sedimentary infill (si), late cement (hc3) [HL 234]; **c:** foraminiferal borings in a wackestone intraclast; **d:** diagenetic sequence with cement 1 (hc1) in intragranular pores, sedimentary infill 1 (si1), cement (hc2), sedimentary infill 2 (si2), late cement (hc3) [HL 234]; **e:** pholadid boring in a wackestone intraclast; **f:** *Otternstella lemmensis* (BERNIER, 1971); **g:** *Aloisalthella sulcata* (ALTH, 1882) inside a black pebble; **h-i:** calpionellids in the coloured micrites [SHJ-10].
All images (a-i) are in optical microscopy transmitted light. a-c, e, g: HL 234; d: SHJ-3Mi; f: SHJ-11; h-i: SHJ-10.
All photographs, except h-i, are at the same scale; white scale bar = 250 µm (a); black scale bar = 100 µm (h-i).

the two planes is approximately 10°, defining a slight angular unconformity and documenting a stratigraphic hiatus. This surface was erroneously interpreted as a hardground (GRANIER, 1987; YÉBENES, 1996; CASTRO JIMÉNEZ, 1998), an interpretation that will be reassessed and discussed in detail later in this paper.

4.2. Biostratigraphy

On one hand, the microfossil assemblage of the Jurassic limestones, comprising calcareous algae [*Aloisalthella sulcata* (ALTH, 1882) (Fig. 4.g; Pl. 1, fig. h; Pl. 5, figs. g *pars*, t, v, w *pars*, x; GRANIER, 1987: Pl. 40, figs. a, d, i-j); *Otternstella lemmensis* (BERNIER, 1971) (Fig. 4.f; GRANIER, 1987: Pl. 33, figs. a, d); *Salpingoporella annulata* (CAROZZI, 1953) (Pl. 5, figs. a-f, g *pars*, h-k; GRANIER, 1987: Pl. 36, fig. i); *Selliporella neocomiensis* (RADOIČIĆ, 1975, non 1963) (GRANIER, 1987: Pl. 41, fig. a); *Thaumatoporella parvovesiculifera* (RAINERI, 1922)] and benthic foraminifers [*Coscinoconus* spp. (Pl. 1, fig. j); *Frentzenella* spp.; *Mohlerina basiliensis* (MOHLER, 1938) (Pl. 5, fig. m); *Pseudocyclammina lituus* (YOKOYAMA, 1890) (Pl. 5, fig. n); *Redmondoides lugeoni* (SEPTFONTAINE, 1977) (Pl. 1, figs. e *pars*, f; Pl. 5, fig. w *pars*; GRANIER, 1987: Pl. 14, fig. g); Trochamminidae ind. (Pl. 1, figs. g, i)], is characteristic of the Tithonian-lower Berriasian interval (see GRANIER, 2019). *Leviathania sautieri* (COQUAND, 1856) (formerly known as *Natica leviathan* PICTET & CAMPICHE, 1863) is also observed, either as isolated specimens or in clusters (Pl. 4, fig. e), at the top of these Jurassic limestones. Although it is commonly cited as indicative of a Berriasian age (Foucault, 1974), the stratigraphic range of this large gastropod remains poorly constrained by biostratigraphic data.

On the other hand, ammonites collected by the first author (BRCG) on 25/07/1984 from the lowermost beds of the ammonite marls include *Macroscaphites yvani* (Puzos, 1832) [formerly known as *Costidiscus recticostatus* (Orbigny, 1840)] (UCBL-FSL 472150), a taxon whose stratigraphic range extends from the upper Barremian to the lower Aptian. The condensed assemblage also comprises *Cheloniceras* spp., including *C.* cf. *cornuelianum* (Orbigny, 1841) (UCBL-FSL 472152), and *Ancyloceras matheronianum* Orbigny, 1842 (UCBL-FSL 471048), which led Granier (1987) to assign these beds to the lowermost Aptian.

On this basis, and by comparison with Cabeçó d'Or and Puig Campana, Granier (1987: p. 218) considered that most of the Berriasian and lowermost Valanginian strata are absent as a result of submarine erosion or abrasion, leaving behind only a few gravel-sized clasts. These are mostly quartz-bearing extraclasts, occurring either as isolated clasts or as nuclei of ferruginous oncoids (Granier, 1987: Pl. 17, figs. c-d), within the condensed interval at the base of the ammonite marls. While the unconformity surface remained largely sediment-free, coloured (pale orange, pink, and red) micrites were deposited below this surface during the remainder of the Valanginian to the Barremian, infilling the pore network of the Jurassic limestones, the voids between breccia clasts, and synsedimentary fractures (*i.e.*, the sedimentary sills). The presence of rare calpionellids in these coloured micrites (Fig. 4.h-i) indicates that their deposition occurred as early as the Valanginian (Granier, 1987: p. 98). In addition to the calpionellids, a few ostracod valves are present in the sedimentary infill of the fractures (Pl. 2, fig. d; enlargement of Pl. 5, fig. o) and some former pores (Pl. 2, figs. e-f) within the Jurassic limestones; these most likely represent the remains of endolithic species.

5. New macroscopic observations and interpretations

Basically, there are two ways to approach and interpret the paleomorphologies of the Jurassic limestones: 1) two-dimensional views along the marine cliff and 2) partial three-dimensional views of their upper surface.

5.1. The marine cliff

Figure 3.b-c shows sigmoidal geometries in the upper part of the Jurassic cliff at Punta de la Pila (Fig. 1.C). Similar geometries are also observed on the cliff west of l'Elefant (Figs. 1.C, 2).

When considered together with the microfacies analysis, which indicates very shallow-water depositional environments during the Tithonian-early Berriasian, these features are interpreted either as sedimentary infill of tidal channels or as the result of lateral accretion of sediments within shallow subtidal to intertidal confined environments favorable to microbial communities (*e.g.*, environments characterized by algal mats, algal films, and oncoid-rich facies).

5.2. The Yébenes paleocave

The identification of a genuine paleocave, *i.e.*, the Yébenes paleocave (Pl. 3, figs. a-c), invalidates Granier's (1987) hypothesis of submarine erosion and abrasion extending downward from the seafloor into the underlying substratum. Instead, it supports the paleokarst hypothesis, implying subaerial exposure and karstic erosion prior to subsequent marine inundation.

The cave is almost entirely filled with sediment (Pl. 3, fig. d; Pl. 4, figs. f-g), including coloured micrites (volumetrically the most significant), angular intraclasts forming chaotic collapse breccias resulting from the collapse and brecciation of the cave roofs, granular material (*e.g.*, crinoid ossicles), and large fossils such as ammonites and belemnites. Locally, the geopetal sedimentary infill displays an hourglass-shaped geometry, resembling sand in an egg timer (Pl. 4, fig. g). This geometry is interpreted as evidence of chimneys in the cave roof that connected the cavity to the seafloor, allowing sediment to be funneled into the cave, like sand through an hourglass. Such chimneys are truncated by the discontinuity surface and can be observed at the top of the Jurassic limestones. Although a few occur as simple subvertical holes (Pl. 3, figs. f-g), most appear as elongated structures (Pl. 3, fig. e) oriented N70°E (WSW-ENE), most likely developed along pre-existing joints ("diaclases" in French) that were subsequently enlarged by dissolution in the vadose zone.

The infills of the dolines (*e.g.*, the doline west of l'Elefant) and of the other caves result from a long and complex history that would require more detailed investigations, which are beyond the scope of the present publication. The Elefant Cave could not be explored because access has been cut off by the evolution of the Morro de Sant Jordi cliff. In the past, the cave was quarried to extract speleothem crystals. However, it can be assumed that the collapse and brecciation were initiated during a meteoric subsurface phase that preceded the marine phreatic environment associated with marine inundation (see next).

5.3. Breccias and sedimentary sills

Breccias and coloured (pale orange, pink, and red) sedimentary sills were first identified by Granier (1987: p. 98, Pl. 13, fig. c; Granier & Perthuisot, 2009, Fig. 2; here Fig. 5) west of l'Elefant (GPS coordinates: 38°33'06.7"N, 0°03'36.8"W); however, they were insufficiently documented. For example, only a single photomicrograph was provided to illustrate their petrographic characteristics (Granier, 1987: Pl. 16, fig. a; Granier & Perthuisot, 2009: Fig. 3).

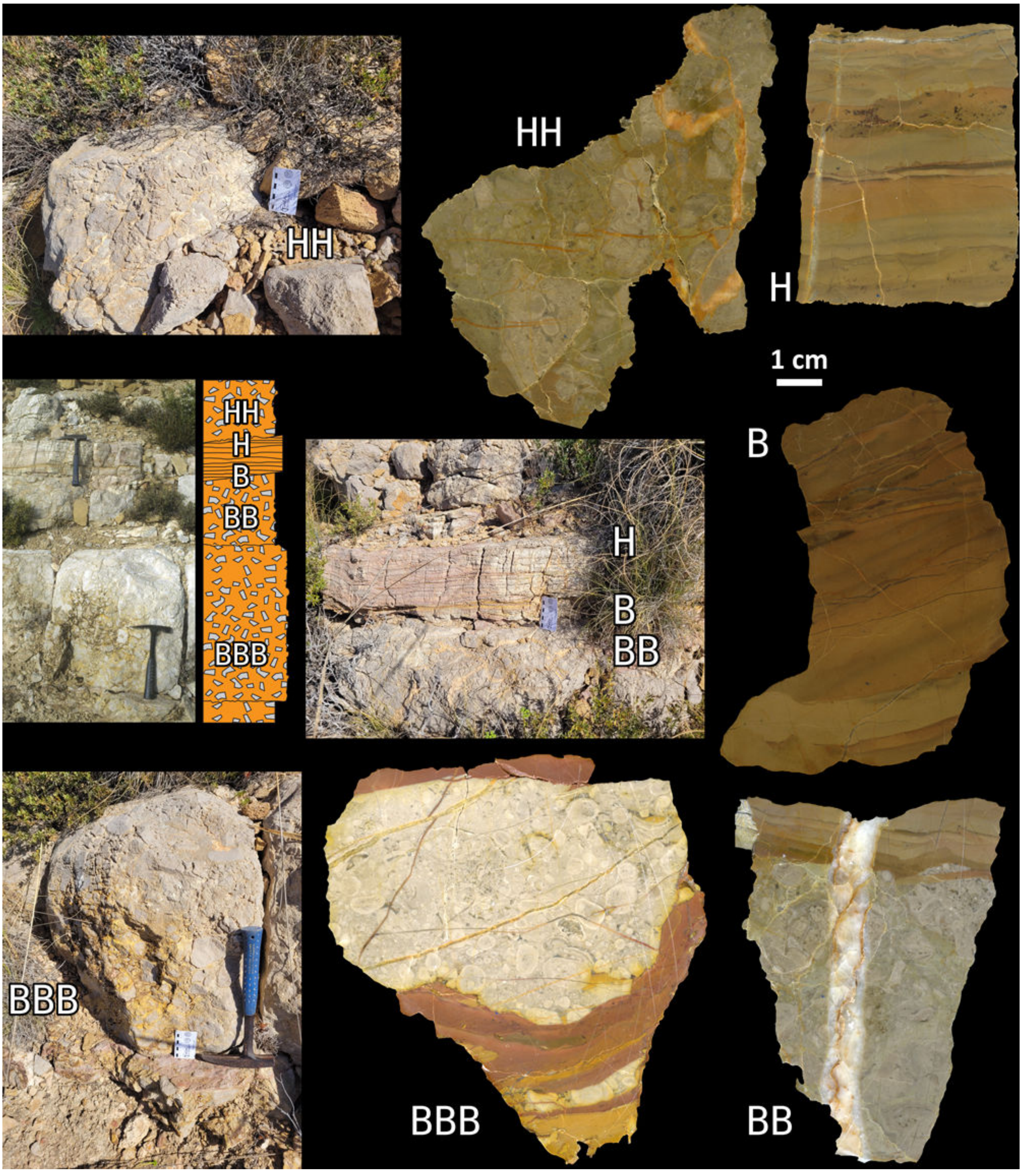

Figure 5: Rock slabs labelled BBB, BB, B, H, and HH, showing chaotic collapse breccia facies, sedimentary sills, and abrupt transitions between them, from a locality situated west of l'Elefant (GPS coordinates: 38°33'06.7"N, 0°03' 36.8"W). The photograph of this small section taken on 28/10/1985 (Granier, 1987: Pl. 13, fig. c) is reproduced here because vegetation cover was less extensive than it is today. The breccia clasts are angular and commonly display irregular outlines. The colored sediment occurring between these intraclasts and within the sedimentary sills, as well as that partially filling intergranular pores within the lithoclasts, consists of micrite showing a geopetal fabric, as can be verified where the cavities are only partially filled (see the largest clast in BBB). The white scale bar on the slabs represents 1 cm.

According to Granier (1987: p. 98), field observations, confirmed by petrographic examination, show that the stratiform coloured layers penetrating the Jurassic limestones correspond to sedimentary infillings of open, subhorizontal fractures. These sedimentary veins were mainly supplied from breccia zones, where gravity-driven coloured sediments accumulated between angular clasts. A secondary contribution resulted from the percolation of sediments through the pore network of the Jurassic limestones with coloured sediments occurring within these small cavities identical in nature to those filling the veins. Locally, thin sparitic cement palisades may delineate a coloured micrite vein. As a result, fracturing, sedimentary infilling, and cementation processes occurred through several successive phases.

GRANIER (1987: p. 219) interpreted the occurrence of these breccias and sedimentary sills as evidence of extensional tectonics affecting the Betic ranges since the Valanginian. However, he did not provide an explanation for the development of the subhorizontal fractures. Once the karstic context is recognized, the opening and subsequent infilling of these fractures become readily understandable. Although local seismicity probably acted as a contributing factor, such fractures are unlikely to have developed in environments lacking large cavities susceptible to collapse.

We previously mentioned the presence of ostracods in cavities (open fractures and pore spaces between breccia clasts) within the Jurassic limestones (Pl. 2, figs. d-f). It is also important to note the occurrence of burrows affecting the micrite of the sedimentary sills (Pl. 2, figs. h-i), which provides additional evidence for the presence of living organisms within submarine cavities.

5.4. The discontinuity surface

The paleokarst hypothesis implies subaerial exposure and erosion.

CASTRO JIMÉNEZ (1998) interpreted the upper surface of the Jurassic limestones as a paleokarst surface ("superficie de paleokarst") characterized by karren features, including solution pans known as kamenitzas. However, this surface lacks the incised morphology typical of true karren field. Instead, it is locally planar, truncating the underlying bedding planes or collapse-breccia pockets. Marine abrasion therefore provides a plausible explanation for the absence of surficial dissolution features.

The mound-and-furrow structures between Cova de Sant Jordi and Cova de l'Elefant (GRANIER, 1987: Pl. 13, fig. b) most likely correspond, respectively, to the host rock and to a collapsed cave or doline (Fig. 3.a). Bluish marls and argillaceous limestones with ammonites overlie in onlap a collapse-breccia facies in this relatively deep and large depression.

Back to Punta de la Pila, the step-like morphology (GRANIER, 1987: Pl. 13, fig. d; CASTRO JIMÉNEZ, 1998: Fig. 3.12.2b) is more likely to represent the steep margin of a broad, shallow depression. However, unlike the smaller depressions, there is no breccia infill but rather sound bedrock at its base. Most likely, wave action removed the sediment that had accumulated within this larger depression, exposing a relatively clean rocky substrate. Both the abrasion surface and the newly exposed, topographically lower surface were subsequently colonized by boring organisms and encrusting biota.

In conclusion, it is suggested here that both karstification and subsequent transgressive abrasion removed a significant volume of rock, while the latter most likely truncated paleocaves and their sedimentary infills, if any.

6. Petrography and microstratigraphy of the pore infills

6.1. Cement stratigraphy

Petrographic analyses focused on sample SHJ-19. Cement types may vary vertically within a single rock sample, as observed in thin section (*e.g.*, Fig. 6.d) or in slab (*e.g.*, Fig. 6.k). Consequently, the sequence of diagenetic events may differ not only within an individual sample but also between samples. Under the standard microscope, thin sections of sample SHJ-19 from above the microbial mat (Fig. 6.b-d, k) display an early cement consisting of a thin isopachous sparite palisade (Fig. 6.a), while the remaining pore space is partly filled with micrite. In contrast, below the microbial mat (Fig. 6.b-d, k), where the oncoids and intergranular pores are larger, early lithification was promoted by yellowish, narrow, fibrous, asymmetric crusts. In addition, early cements are represented by cloudy sparite (Fig. 6.e-j, l-m) containing ghosts of pre-existing structures (*e.g.*, Fig. 6.g-h). Toward the centre of the pores, these cloudy crystals transition abruptly to clear, hyaline sparite (Fig. 6.e-j, l-m). Unlike the hyaline sparite, the cloudy sparite exhibits a pitted appearance under the scanning electron microscope, reflecting the presence of impurities within its crystals (Pl. 6, fig. h). Locally, coloured (pale orange, pink, and red) geopetal micritic sedimentary infills are intercalated into the above-described cement sequence during the hyaline cementation phase. These micritic sediments are similar to those that fill the voids between breccia clasts and the contemporaneous fractures, as well as those occurring in the ferruginous ooid-oncoid floatstones to wackestones. Assuming they are time-equivalent to the condensed sections at Puig Campana and Cabeçó d'Or, GRANIER (1987, p. 98) assigned them a Valanginian (*pro parte*) to early Aptian (*pro parte*) age.

Under cathodoluminescence, the yellowish crusts and the overlying cloudy sparite bands are predominantly non-luminescent (brown to light brown or dark blue to brown dark, depending on the exposure) and lack discernible crystal boundaries. They may exhibit faint zoning, although their texture is mainly patterned with scattered yellow luminescent spots. The contact between the cloudy sparite and the hyaline sparite, which fills the remaining pore space, is irregular. In contrast to the cloudy sparite, the hyaline sparite consists of euhedral crystals. Under cathodoluminescence, these crystals are zoned, initially displaying alternating thick black and thinner brown luminescent bands before becoming predominantly brown luminescent with a medial bright yellow luminescent band.

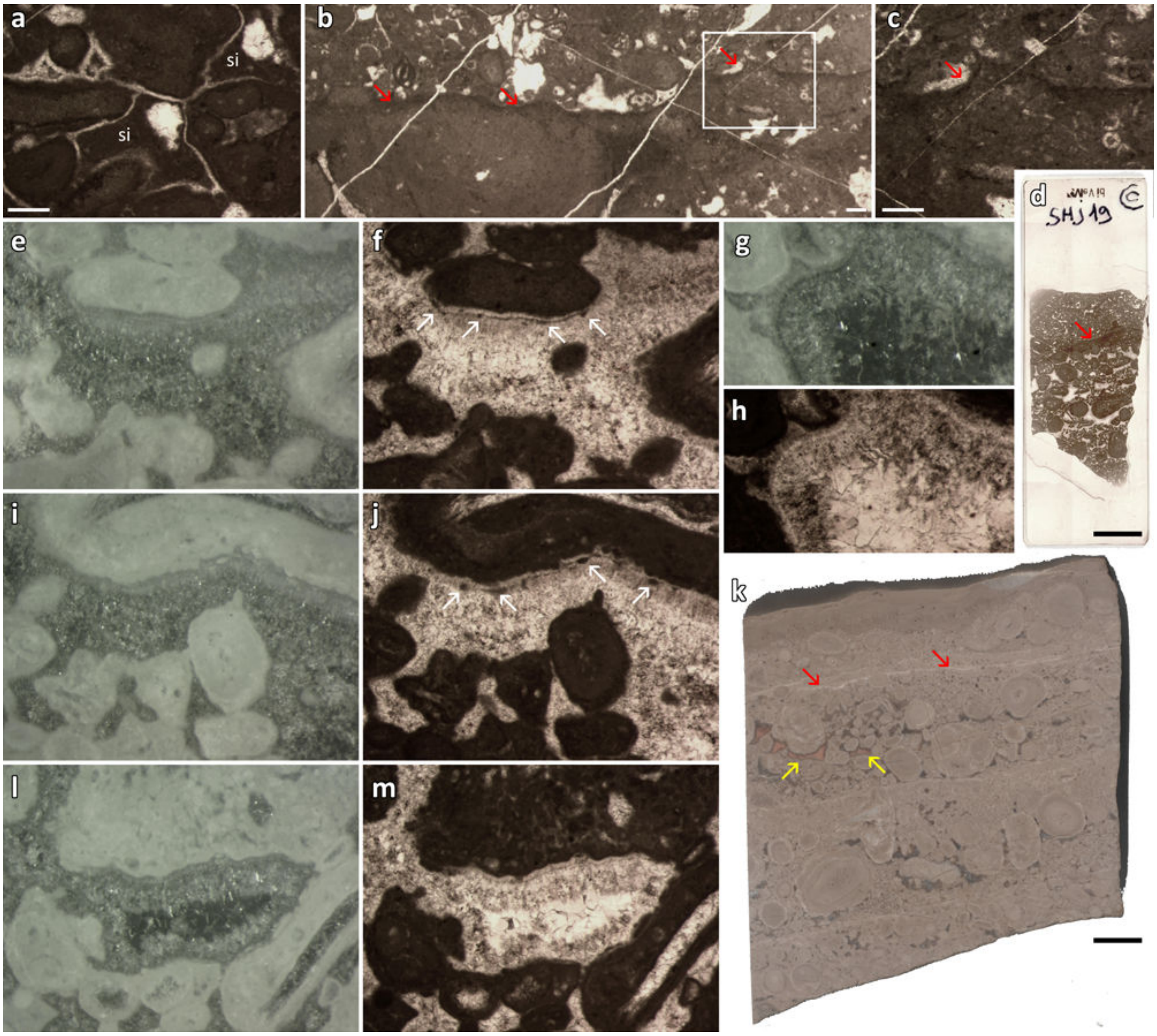

Figure 6: Morro de Sant Jordi. Material from sample SHJ-19, **a:** early isopachous palisade calcite cement fringing allochems and later geopetal micritic sedimentary infill (si) of the intergranular pores; **b-c:** micritic microbial film (red arrows); **d:** the thin section; **e-f, i-j, l-m:** thin endostromatolitic crust composed of micritic clots (white arrows), overlain by calcite crystals that are initially cloudy spar and become hyaline toward the centers of the pores; **g-h:** possible meniscus cement preceding the precipitation of the cloudy sparry calcite cement; **k:** polished slab showing several microbial films (*e.g.*, red arrows) and sparse sedimentary infills of intergranular pores by coloured micrite (yellow arrows).
All images (a-i) were obtained by transmitted-light optical microscopy: images a-c, f, h, j, and m in transmitted light; images e, g, i, and l in reflected light.
All photographs, except b, d, and k, are at the same scale. White scale bar = 250 µm; black scale bar in d and k = 1 cm.

Where present, micritic sedimentary infills were deposited before the formation of the bright yellow luminescent band and are enclosed within the lower part of the predominantly brown-luminescent zone. Closer examination of the crystal zonation reveals a subtle change at a slightly corroded zonal boundary that coincides with the micrite deposition. This boundary also marks a slight change in crystal growth orientation that occurred when cement overgrowth resumed after the deposition of the micritic infill.

In some samples, crystal zonation can also be visible under the standard microscope as a coloured band (*e.g.*, Pl. 5, figs. r-s) and under the scanning electron microscope either as a darker band within the crystals (*e.g.*, Pl. 6, figs. d-e) or dissolution zoning of some crystals on the polished, then slightly etched surface (*e.g.*, Pl. 7, fig. e).

The early cement above the microbial mat in Sample SHJ-19 (Fig. 6.b-d, k), consisting of a thin isopachous sparite palisade (Fig. 6.a), is indicative of precipitation within a phreatic diagenetic zone, which could have been either a marine or a meteoric environment.

Below the microbial mat (Fig. 6.b-d, k), the yellowish asymmetric crusts observed on some allochems are most likely thin endostromatolites (Fig. 6.f, j, m). The presence of micritic clots within these organically pigmented crusts (arrowed in Fig. 6.f, j) supports this interpretation.

The earliest true (chemical) cement is represented by cloudy sparite, which may form a relatively thick, symmetrical cement rim (Fig. 6.e-j, l-m). Based on its cathodoluminescence characteristics (namely its patterned texture, scattered yellow luminescent spots, and wavy outer boundary), this cement rim most likely formed through the recrystallization (*sensu* Saller, 2024) of an original aragonite or high-Mg calcite cement. If so, it indicates precipitation within the marine phreatic diagenetic zone. The overlying hyaline sparite represents a low-Mg calcite cement that may have precipitated in diagenetic environments ranging from the meteoric phreatic zone to the deep-burial realm. Based on the cement stratigraphy, and in particular on the timing of the coloured micritic infills, and on crystal morphology, the hyaline sparite that predates these infills is interpreted as having precipitated within the dominantly oxidizing meteoric phreatic diagenetic zone. The slight corrosion observed at a crystal-zoning boundary within the hyaline sparite coincides with a micritic infill. The micritic particles, composed of relatively deep-water coloured sediment, were transported with seawater through percolation. Accordingly, the corrosion feature is interpreted to reflect a brief episode of water mixing. The medial bright yellow luminescent band that follows the micritic infill may record a seawater-recharge event affecting the phreatic aquifer with stagnant to reducing conditions. It may, therefore, be inferred with reasonable confidence that the transition from crystal growth under meteoric phreatic conditions to growth in the deep-burial realm took place near this medial luminescent band. The study of micritic envelopes under a standard petrographic microscope (Fig. 4.b; Pl. 5, fig. q) reveals that the aragonite shells were not leached during the synsedimentary or early post-sedimentary stage (*i.e.*, as in beachrocks), but rather at a later diagenetic stage. In the first photomicrograph discussed here (Fig. 4.b), the microfacies exhibits a mud-supported fabric, and the primary porosity was predominantly intragranular. The spiral cavity of the gastropod shell was partly cemented by a relatively thick isopachous cement (hc1), consisting of an initial cloudy fringe followed by a hyaline fringe. Dissolution of the aragonitic shell postdated this early cementation phase (hc1). It was followed by a relatively thin generation of hyaline cement (hc2), which lined the moldic pore or formed an overgrowth of the first hyaline cement (hc1) within the shell lumen. A micritic sedimentary infill (si) postdates this second cement phase (hc2); it partly fills the shell lumen and completely fills the large moldic cavity. Cement phase hc1 most likely represents an early marine to meteoric phreatic cement, whereas hc2 corresponds to a meteoric phreatic cement. The final cement generation (hc3), which occludes all remaining pores, most likely represents meteoric phreatic to burial cement.

In the second photomicrograph discussed here (Pl. 5, fig. q), the microfacies has a grain-supported fabric and primary porosity was predominantly intergranular. Dissolution of the aragonitic gastropod shell occurred after precipitation of a circumgranular hyaline cement (hc1). It was followed by precipitation of a second generation of hyaline cement with a dog-tooth habit (hc2), which lines the moldic pore and locally forms an overgrowth on the first hyaline cement (hc1) within the remaining intergranular pore network. Locally, a first micritic sedimentary infill (si1) occurs between the two cement generations, whereas a second micritic sedimentary infill (si2) fills the moldic pore above, and therefore postdates, the second cementation phase (hc2). Cement phase hc1 is most likely an early marine cement, whereas hc2 represents a meteoric phreatic cement. The final cement phase (hc3), which occludes all remaining pores, most likely corresponds to meteoric phreatic to burial cement.

6.2. Borings

It is important to note that borings are not exclusive diagnostic features of hardgrounds. Although the upper surface of the Jurassic limestones is locally bored, it does not constitute a hardground but rather represents a bored rocky substrate, *i.e.*, partly a hard-rock terrace.

In fact, hardgrounds *sensu* Shearman (2025) form on the seafloor through early marine cementation, typically within grain-supported fabrics. There, isopachous rims of aragonite needles or high-Mg calcite fibres precipitate within the intergranular pore network, generally to depths of a few centimeters to decimeters below the seafloor within the marine phreatic zone.

The occurrence of borings alone is, therefore, insufficient to identify a hardground, as they may develop on a variety of hard substrates, including intraclasts (Fig. 4.a, e), oncoids, corals, and large shells (Granier, 2021).

At Punta de la Pila, the surface is, instead, interpreted as an abrasion surface produced during marine flooding of the karstified rocky shore of the Serra Gelada paleo-island. The surface was subsequently colonized by boring organisms.

6.3. Calcarenite extraclasts

As a side consideration, although the small extraclasts found in the lowermost part of Unit 6 or in the sedimentary sills (see Granier, 1987: Pl. 17, figs. c-d) were initially interpreted as being derived from lower Valanginian calcarenites with *Pseudocyclammina* (Unit 5), this was most likely a misidentification. Since no remnants of Units 3-5 have been identified at Serra Gelada, these small extraclasts (Pl. 2, figs. j-k) most likely originated from the middle Berriasian sandstones and oolites with *Ichnusella* (Unit 2). Other extraclasts are found to originate from Unit 1: for instance, in the condensed section at the base of the ammonite marls, we found a small extraclast acting as the nucleus of a ferruginous oncoid (Pl. 2, fig. l).

At Puig Campana, the abrupt transition from high-energy sandstones and oolites with *Ichnusella* (Unit 2) to low-energy marls with *Falsolikanella* and charophytes (Unit 3) marks a major downward shift in facies (see GRANIER, 1987: Fig. 40). This transition suggests that the associated subaerial exposure and subsequent karstification observed at Serra Gelada were coeval to this specific relative sea-level fall and most likely occurred during the late Berriasian to early Valanginian, an interval when shallow-water environments prevailed at Puig Campana and Cabeçó d'Or. Considering the measured angular unconformity and the disappearance of the Berriasian sandstones and oolites with *Ichnusella* (Unit 2) over a distance of 2 km (from Isleta Mitjana to Morro de Sant Jordi), it is most likely that the emergence is not necessarily related to a negative eustatic pulse but to a very localized substratum rise, the motor of which - considering the local geological setting - was most likely salt tectonics.

6.4. Estimating the missing time at the discontinuity

Petrographic and micropaleontological analyses of the few samples collected from the uppermost strata at Isleta Mitjana revealed that they do not consist of Tithonian-lower Berriasian limestones with *Aloisalthella* (Unit 1), as at Morro de Sant Jordi, but rather of middle Berriasian sandstones and oolites with *Ichnusella* (Unit 2). In addition to silt- to sand-sized quartz grains and ooids, the allochems comprise bioclasts, including microfossils such as *Coscinoconus* spp. (Pl. 1, fig. c), "*Macroporella*"? *praturloni* (DRAGASTAN, 1978, non 1971) (Pl. 1, fig. a), and *Marinella lugeoni* PFENDER, 1939 (Pl. 1, fig. b; see GRANIER & DIAS-BRITO, 2016).

GRANIER (1987) assigned the first beds capping the Jurassic to the lowermost Aptian. However, on 22/09/2010, R. BUSNARDO collected several specimens of *Barremites* spp. (UCBL-FSL 471050), confirming the presence of latest Barremian taxa within the basal condensed interval. Nevertheless, the submersion of the Serra Gelada paleo-island cannot be ascribe to this age because, below the unconformity surface, within the rocky Jurassic substratum, the coloured (pale orange, pink, and red) micrites infilling the porous network (intergranular pores, dissolution cavities from microscopic to metric in dimensions, fractures) also represent deep-marine deposits. By analogy with the condensed intervals of Puig Campana and Cabeçó d'Or, and considering the presence of Calpionellids in some coloured micritic sedimentary sills, together with the abrupt deepening associated to the onset of an extensional tectonic phase dated to the early Valanginian, these deposits most likely accumulated during the Valanginian *pro parte* to the Barremian.

7. Conclusions

According to the observations presented above, several aspects of the local geohistory can be reconstructed.

The abundance and diversity of calcareous green algae in the Tithonian-lower Berriasian limestones of Unit 1 indicate deposition in shallow-water, most likely subtidal to intertidal environments less than 10 m deep. This interpretation is supported by numerous sedimentary features observed at various scales, including fenestrae and possible keystone vugs, algal-microbial films, possible black pebbles, and tidal-channel or lateral-accretion structures. Collectively, these observations rule out the previous interpretation of these deposits as mud-mound facies. In retrospect, that interpretation was biased by the limited sedimentological evidence then available and is not supported by the present data.

As at the nearby Puig Campana and Cabeçó d'Or, Unit 1 is overlain by the transgressive middle Berriasian calcarenites and oolites of Unit 2. Owing to subsequent erosion, Unit 2 is preserved only at Isleta Mitjana. At Morro de Sant Jordi, it is absent, with only a few sandstone gravels representing its last vestiges, which the first author (BRCG) previously and erroneously interpreted as being reworked from Unit 5. Whereas Unit 3, including charophyte-bearing marls, was deposited in the nearby Puig Campana and Cabeçó d'Or areas, the combined effects of forced regression and, most probably, very localized salt tectonics during the middle-late Berriasian transition led to the emergence of the Serra Gelada area. A similar phenomenon was observed later, during the Albian, in the Cabeçó d'Or area (GRANIER *et al.*, 2025). In addition, at Serra Gelada, although the evaporite series associated with the nearby Altea diapir began to flow during the Eocene, prior to its extrusion in the Oligocene (RÍOS GARCÍA *et al.*, 1960; NAVARRO *et al.*, 1962; MOSELEY *et al.*, 1985; RUIG, 1995; HERNÁNDEZ SAMANIEGO *et al.*, 2008), evidence for even earlier salt flows was provided by the reworking of Triassic material (*i.e.*, authigenic quartz with anhydrite inclusions) within Albian strata (GRANIER, 1987: Pl. 25, figs. d-h; GRANIER & PERTHUISOT, 2009: Fig. 6).

Throughout the late Berriasian and early Valanginian, corresponding to the deposition of Units 3 to 5 at Puig Campana and Cabeçó d'Or, the Serra Gelada area remained subaerially exposed. During this interval, karst features, including chimneys, dolines, and caves, developed, and some caves underwent partial collapse. Karstification resulted in variable degrees of chemical dissolution of the Jurassic limestones within the meteoric vadose zone, the presence of which is documented at multiple scales, from thin-section to outcrop scale. This karstification was accompanied by the development of a Ca-rich, non-marine phreatic groundwater system.

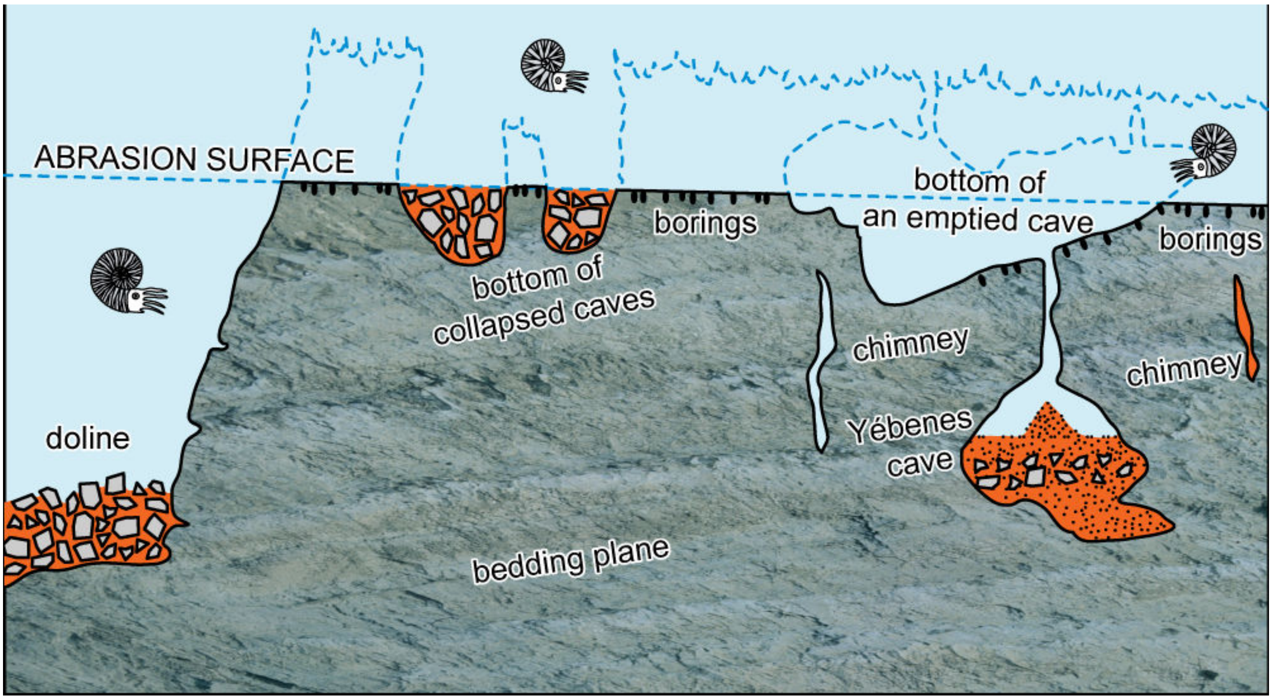

Figure 7: Model of the Morro de Sant Jordi sea cliff, including the Valanginian abrasion surface, the YÉBENES Cave, the chimneys, and the emptied cave floor at Punta de la Pila, as well as the l'Elefant doline.

Consequently, non-luminescent drusy calcite cements precipitated within this phreatic zone, partly occluding the intergranular pore network. Given its location far from the paleoshoreline and the relatively continuous marine sedimentary record preserved the intervening area, represented by the sections at Puig Campana and Serra de Mariola, Serra Gelada must have formed an isolated paleo-island during this interval.

Major block faulting related to the extensional tectonic and deepening phase began during the late early Valanginian (GRANIER, 1987; GRANIER & PERTHUISOT, 2009). At Puig Campana and Cabeçó d'Or, the signature of the associated deepening phase is marked by an abrupt facies change from high-energy calcarenites with hummocky and swaley cross-stratifications of the Unit 5 to condensed successions dominated by low-energy micritic sediments of the Unit 6. There, although these successions locally include ferruginous crusts that may have served as a hard substrate for worm tubes, they typically consist of a basal silty and sandy calpionellid wackestone overlain by ferruginous oolitic wackestones to oncolitic floatstones with ammonites, themselves succeeded by glauconitic wackestones. The silty and sandy calpionellid wackestone resulted from the bioturbation-induced mixing of quartzitic material derived from the uppermost strata of Unit 5 with the micrite from the lowermost strata of Unit 6. Thus, no hardground developed at the boundary. At Serra Gelada, only ferruginous crusts and ferruginous oolitic wackestones to ferruginous oncolitic floatstones are present.

The submergence of the former island led to the development of a wave-cut terrace during the Valanginian. Its erosional surface truncates the pre-existing karstified rocky substrate of Serra Gelada paleo-island, including paleocaves and their infills, if any (Fig. 7). From the Valanginian and into the Hauterivian and Barremian (not into the earliest Aptian as previously inferred), sedimentation was restricted to the gravitational percolation of coloured micrites into synsedimentary fractures, chimneys, and the interconnected pore network of the intact Jurassic bedrock and associated collapse breccias. Following the flooding of the paleo-island, the associated late Berriasian-early Valanginian captive meteoric lens was locally affected by minor ingressions of marine water accompanying the downward percolation of micritic sediment. This resulted in limited corrosion of the meteoric phreatic cement. Later in the cementation sequence, the yellow-luminescent band visible in cathodoluminescence imagery records an abrupt shift in the hydrochemistry of the meteoric aquifer. This change is interpreted to have resulted from faulting and the development of open fractures, which facilitated the ingress of marine-derived fluids. The fracturing and brecciation are polyphase, as demonstrated by cross-cutting relationships between successive phases of marine phreatic cementation and sedimentary infilling. Subsequently, during burial diagenesis, the pore brine became progressively homogenized.

In summary, although further advances in understanding the sequence of events may still be achieved, notably through a detailed study of the paleokarst system and its infilling, the results presented here - based on integrated observations and interpretations - represent a major step forward in understanding the processes that affected this area. They not only refine the interpretation of local events but also provide new insights at the regional scale, through the identification of a paleo-island located nearly 50 km from the late Berriasian-early Valanginian paleo-shoreline (northwest of the Serra de Mariola). This island emergence was most likely related to a process of salt diapirism involving Triassic evaporites, which currently represents the only plausible mechanism capable of explaining positive tectonic movement of the marine substrate at that time. The study also reveals the existence of a paleokarst network that developed contemporaneously with the emergence phase. Its complex sedimentary infill - comprising cave-collapse breccias and marine deposits - was emplaced mainly after the island was submerged, during the mid-Valanginian extensional tectonic phase, and continued until the end of the Barremian.

Acknowledgements

The Parque Natural de la Serra Gelada granted permission to access the cliffs, for which we are grateful.

Because the Jurassic and lowermost Cretaceous exposures at Morro de Sant Jordi and Isleta Mitjana are only accessible by sea, fieldwork was highly dependent on weather conditions and the availability of boats and skippers. We are sincerely grateful to Jaume FUSTER, owner of the Marraix, who kindly transported three of us (BRCG, JETM, and DB) to Isleta Mitjana on 11 November 2025. More recently, on 15-16 June 2026, the same team conducted fieldwork aboard the Ephira (funded by Sea4Future project), the vessel of the Laboratorio Marino UA-Dénia, a branch of the Instituto Multidisciplinar Ramón MARGALEF of the University of Alicante, in order to reach Morro de Sant Jordi. We thank its director, Dr César BORDEHORE FONTANET, as well as the skippers John Antony YAÑEZ DOBSON and Jaime FERNÁNDEZ DEL CAMPO, and our accompanying colleague Daniela DE LA ROCHA, for their valuable assistance. Mooring of the Ephira was kindly provided by the Club Náutico de Altea, which is gratefully acknowledged for the use of its facilities.

The first author (BRCG) gratefully acknowledges the Department of Earth and Environmental Sciences, University of Alicante (San Vicente del Raspeig), for hosting him on two occasions, from 14 to 24 November 2025 and from 12 to 22 June 2026, within the framework of the VIGROB-053 project. This research was supported by the Spanish Ministry of Science and Innovation (Research Project PID2025-167899NB-I00). Additional expenses were covered by a grant from the Association Carnets de Géologie.

Technical support for this work was provided by both the University of Alicante and the Nanjing Institute of Geology and Palaeontology, Chinese Academy of Sciences, where the first author (BRCG) was hosted under the President's International Fellowship Initiative (PIFI) and conducted research from 3 March to 3 May 2026.

The UCBL-FSL-numbered ammonites are part of the "Collections de l'Université Claude BERNARD Lyon 1" (GRANIER Collection), Villeurbanne, France. The studied thin sections and polished slabs will be deposited in the collections of the Muséum d'Histoire Naturelle de Genève, Switzerland.

Special thanks are extended to Mohamed BENZAGGAGH and Didier BERT for their valuable insights on calpionellids and ammonites.

We sincerely thank the editor, Jordi PÉREZ-CANO, and the four reviewers, Telm BOVER-ARNAL, Ioan BUCUR, Cristian V. MIRCESCU, and Robert W. SCOTT, for their careful evaluation of the manuscript and for their constructive and helpful comments, which have contributed to improving the paper.

Bibliographic references

ALTH A. von (1882).- Die versteinerungen des Niźniower Kalksteines.- *Beiträge zur Paläontologie Österreich-Ungarns und des Orients*, Wien, Band I, p. 183-332.

BERNIER P. (1971).- Deux nouvelles algues dasycladacées du Jurassique supérieur du Jura méridional.- Géobios, vol. 4, no. 3, p. 173-184.

CAROZZI A. (1953).- Découverte du genre *Salpingoporella* dans le Jurassique supérieur du Grand Salève.- *Archives de la Société de Physique et d'Histoire naturelle*, Genève, vol. 6, fasc. 6, p. 382-386.

CASTRO JIMÉNEZ J.M. (1998).- Las plataformas del Valanginiense superior-Albiense superior en el Prebético de Alicante.- Tesis Doctoral, Universidad de Granada, xiv + 452 p. (XIX Pls.).

COQUAND H. (1856).- Description de quelques espèces nouvelles de coquilles fossiles découvertes dans la chaine du Jura.- *Mémoires de la Société d'émulation du Département du Doubs* (deuxième série), Besançon, vol. 7, p. 45-50. URL: https://www.biodiversitylibrary.org/page/37110197

DRAGASTAN O. (1971).- New Algae in the Upper Jurassic and Lower Cretaceous in the Bicaz valley (East Carpathians) Romania.- *Revista Española de Micropaleontología*, Madrid, vol. III, p. 155-192.

DRAGASTAN O. (1978).- Microfaciès de la série calcaire, crétacée inférieure d'Aliman (Drobrogea de Sud).- *Dări de seamă ale sedintelor* (4. Stratigrafie), Bucureşti, vol. LXIV (1976-1977), p. 107-136.

FOUCAULT A. (1974).- L'âge d'*Ampullina* (ex *Natica*) *leviathan* précisé en Espagne du Sud (zone prébétique) grâce à des Calpionelles (Berriasien et Berriasien-Valanginien inférieur).- *Boletín Geológico y Minero*, Madrid, t. LXXXV-I, p. 4-9.

FUSTER Jaume & FUSTER Joan (2017).- La Torre de Las caletas. A la vora de l'abisme.- Ayuntamiento de Benidorm, Festes Majors Patronals de Benidorm, la Taula del Bon Profit, 32 p.

GRANIER B. (1987).- Le Crétacé inférieur de la Costa Blanca entre Busot et Altea, Alicante (Espagne) : Biostratigraphie, sédimentologie, évolution tectono-sédimentaire.- Thèse, Docteur de l'Université Paris VI (nouveau régime), 23

Novembre 1987; *Mémoires des Sciences de la Terre, Université Pierre et Marie Curie*, Paris, no. 87-49, vol. I (text): 281 p.; vol. II (plates): 54 pls. URL: https://hal.science/view/index/docid/5723936

GRANIER B. (2019).- Dual biozonation scheme (benthic foraminifera and "calcareous" green algae) over the Jurassic-Cretaceous transition. Another plea to revert the system boundary to its historical ORBIGNY's and OPPEL's definition. *In*: GRANIER B. (ed.), VSI: The transition of the Jurassic to the Cretaceous: An early XXIth century holistic approach.- *Cretaceous Research*, vol. 93, p. 245-274.

GRANIER B. (2020).- The biosignature of sparite permits the distinction between gravitational cement and endostromatolites.- *Carnets Geol.*, Madrid, vol. 20, no. 20, p. 407-419. DOI: 10.2110/carnets.2020.2020

GRANIER B.R.C. (2021).- *Bacinella*, a discrete type of Mesozoic calcimicrobial structure.- *Carnets Geol.*, Madrid, vol. 21, no. 1, p. 1-25. DOI: 10.2110/carnets.2021.2101

GRANIER B. & DIAS-BRITO D. (2016).- On the fossil alga *Marinella lugeoni* PFENDER, 1939, *nom. cons.*, and its seven unfortunate avatars. Revision of the Juliette PFENDER Collection. Part 2. Revision of the Jesse Harlan JOHNSON Collection. Part 2.- *Carnets Geol.*, Madrid, vol. 16, no. 7, p. 231-245. DOI: 10.4267/2042/59922

GRANIER B. & LETHIERS A. (2019).- *Aloisalthella*, a new fossil Polyphysacean genus (Chlorophyta, Dasycladales), and its allied genus *Clypeina* (MICHELIN, 1845).- *Palaeontologica Electronica*, article 22.2.45, 20 p. DOI: 10.26879/923

GRANIER B. & PERTHUISOT V. (2009).- Discussion of: Development of carbonate platforms on an extensional (rifted) margin: the Valanginian-Albian record of the Prebetic of Alicante (SE Spain), by J.M. CASTRO *et al.*, Cretaceous Research 29 (2008), 848-860.- *Cretaceous Research*, vol. 30, p. 1019-1026.

GRANIER B.R.C., ROBERT E. & PÉREZ-MALO J. (2025).- The Aptian-Albian of the Costa Blanca (SE Spain): Implications for identifying the Aptian/Albian boundary in the neritic zone within the Tethys realm.- *Carnets Geol.*, Madrid, vol. 25, no. 5, p. 109-145. DOI: 10.2110/carnets.2025.2505

HERNÁNDEZ SAMANIEGO A., NAVARRO JULI J.J., PASCUAL MUÑOZ H., ESTÉVEZ RUBIO A. & LÓPEZ ARCOS M. (2008).- Hoja 848 (Benidorm), 30-33.- *Mapa geológico de España*, Madrid, Escala 1:50.000, Secunda serie, Primera edición, Memoria asociada al mapa de la hoja 848, 73 p. URL: https://info.igme.es/cartografiadigital/geologica/Magna50Hoja.aspx?language=es&id=848

LEUPOLD W. & BIGLER H. (1936).- *Coscinoconus* eine neue Foraminiferenform aus Tithon-Unterkreide-Gesteinen der Helvetischen Zone der Alpen.- *Eclogae Geologicae Helvetiae*, Basel, Band 28, p. 606-624 (Pl. XVIII). URL: https://www.e-periodica.ch/digbib/view?pid=egh-001:1935:28#668

MOHLER W.A. (1938).- Mikropaläontologische Untersuchungen in der nordschweizerischen Juraformation.- *Abhandlungen der Schweizerischen Paläontologischen Gesellschaft*, Basel, Band 60, p. 1-53.

NAVARRO A., TRIGUEROS E., VILLALÓN C. & RÍOS J.M. (1962).- Derniers progrès dans la connaissance de l'extrémité nord-est des Chaînes subbétiques (Région d'Altea-Benissa, province d'Alicante, Espagne). *In*: Livre à la mémoire du Professeur P. FALLOT.- *Mémoire hors-série de la Société géologique de France*, Paris, p. 143-153.

ORBIGNY A. d' (1840-1842).- Paléontologie française, terrains crétacés, I - Céphalopodes.- Masson, Paris, 662 p. (148 Pls.). URL: http://www.biodiversitylibrary.org/page/22587199 (texte); http://www.biodiversitylibrary.org/page/20516109 (Atlas)

PFENDER J. (1939).- Sur un calcaire phytogène du Lias inférieur d'Espagne et l'extension de ce faciès en quelques autres régions.- *Bulletin de la Société vaudoise des Sciences naturelles*, vol. 60, no. 248, p. 213-228 (Pls. I-V).

PICTET F.-J. & CAMPICHE G. (1861-1864).- Description des fossils du terrain Crétacé des environs de Sainte-Croix. Deuxième partie.- H. Georg, Genève, 752 p., Pls. 44-98 [1861, 1-3: 1-144, Pls. 44-57; 1862, 4-7: 145-349, Pls. 58-76; 1863, 8-10: 350-524, Pls. 77-89; 1864, 11-12: 525-752, Pls. 90-98]. URL: https://www.biodiversitylibrary.org/page/36420499

PUZOS M. (1832).- *Scaphites Yvanii*. Séance du 19 Mars 1832.- *Bulletin de la Société Géologique de la France*, Paris, tome second, p. 355-356 (Pl. II). URL: http://www.biodiversitylibrary.org/page/53829474

RADOIČIĆ R. (1963).- *Triploporella neocomiensis* spec. nov. iz slojeva valendis-otriva Crne Gore (*Triploporella neocomiensis* spec. nov. des couches valanginiennes-hau-tiriviennes du Montenegro).- *Vesnik (Geologija* (serie A)*)*, Beograd, vol. XXI, p. 139-144.

RADOIČIĆ R. (1975).- *Linoporella buseri* sp. nov. from the Liassic of the Julian Alps (a preliminary report).- *Bulletin Scientifique, Conseil des Academies des Sciences et des Arts de la RSF de Yougoslavie* (Section A: Sciences Naturelles, Techniques et Medicales), Zagreb, vol. 20, p. 277-278.

RAINERI R. (1922).- Alghe sifonee fossili della Libia.- *Atti della Società Italiana di Scienze Naturali e del Museo Civico di Storia Naturale di Milano*, vol. LXI, fasc. 1, p. 72-86. URL: http://www.biodiversitylibrary.org/page/57807523

RIGAUD S., BLAU J., MARTINI R. & RETTORI R. (2013).- Taxonomy and phylogeny of the Trocholinidae (Involutinina).- *The Journal of Foraminiferal Research*, vol. 43, no. 4, p. 317-339.

RIGAUD S., SCHLAGINTWEIT F. & BUCUR I.I. (2018).- The foraminiferal genus *Neotrocholina* REICHEL, 1955 and its less known relatives: A reappraisal.- *Cretaceous Research*, vol. 91, p. 41-65.

Ríos García J.M., Villalón Dávila C., Trigueros Molina E. & Navarro Alvargonzález A. (1960).- Hoja 848 (Altea).- *Mapa geológico de España*, Madrid, Escala 1:50.000, Primera serie, Memoria asociada al mapa de la hoja 848, 98 p. URL: https://info.igme.es/cartografiadigital/geologica/Geo50Hoja.aspx?intranet=false&id=848

Ruig M.J. de (1995).- Chapter 17. Extensional diapirism in the Eastern Prebetic foldbelt, southeastern Spain. *In*: Jackson M.P.A., Roberts DG. & Snedson S. (eds.), Salt tectonics: A global perspective.- *AAPG Memoir*, Tulsa - OK, vol. 65, p. 353-367.

Saller A. (2024).- Aragonite neomorphism via intrafabric dissolution and calcite precipitation, not thin films.- *Carnets Geol.*, Madrid, vol. 25, no. 1, p. 1-28. DOI: 10.2110/carnets.2025.2501

Septfontaine M. (1977).- Niveaux à Foraminifères (Pfenderininae et Valvulininae) dans le Dogger des Préalpes médianes du Chablais occidental (Haute-Savoie, France).- *Eclogae Geologicae Helvetiae*, Bâle, vol. 70, no. 2, p. 599-625. DOI: 10.5169/seals-164631

Shearman D.J. (2025).- Laboratory handbook of carbonate petrology.- Carnets de Géologie, Madrid, CG2025_B01, iv + 55 p. DOI: 10.2110/carnets.2025.0001

Verneuil É. de & Collomb É. (1853).- Coup d'œil sur la constitution géologique de quelques provinces de l'Espagne.- *Bulletin de la Société Géologique de la France* (2e série), Paris, t. X, p. 61-147. URL: http://www.biodiversitylibrary.org/page/54358104

Yébenes A. (1996).- Estratigrafía y estructura de la Sierra Gelada.- *Cuadernos de Geografía de la Universitat de València*, no. 60, p. 201-222. URL: https://turia.uv.es/index.php/CGUV/en/article/view/14704

Yokoyama M. (1890).- Foraminiferen aus dem Kalksteine von Torinosu und Kompira.- *Denkschriften der Kaiserlichen Akademie der Wissenschaften* (Mathematisch-Naturwissenschaftliche Classe), Wien, Band 57, p. 26-27. URL: http://www.biodiversitylibrary.org/page/7128731

Zaninetti L. (1978).- Un organisme *incertae sedis* nouveau dans le Permien supérieur du Sud Zagros, Iran.- *Note du Laboratoire de Paléontologie de l'Université de Genève*, vol. 3, p. 17-19.

Plates

Plate 1: figs. a-d: Isleta Mitjana: **fig. a:** "*Macroporella*"? *praturloni* (Dragastan, 1978, non 1971); **fig. b:** *Marinella lugeoni* Pfender, 1939; **fig. c:** *Coscinoconus alpinus* Leupold *in* Leupold & Bigler, 1936; **fig. d:** *Aloisalthella sulcata* (Alth, 1882) reworked from Unit 1 into unit 2; **figs. e-q:** Morro de Sant Jordi: **fig. e:** *Redmondoides lugeoni* (Septfontaine, 1977) and *Cayeuxia*-like structures; **fig. f:** *Redmondoides lugeoni* (Septfontaine, 1977); **figs. g, i:** Trochamminidae ind.; **fig. h:** *Aloisalthella sulcata* (Alth, 1882); **fig. j:** *Coscinoconus alpinus* Leupold *in* Leupold & Bigler, 1936; **figs. k-q:** *Cayeuxia*-like structures occurring as components of the boundstone (k-m), as discrete allochems (o-q), or attached to an oncoid (n).
All images (a-i) were obtained by transmitted-light optical microscopy. a: MIT-3; b-d: MIT-4; e, l-m, p-q: SHJ-2; f, h: SHJ-3Mi; g: SHJ-3H; i: SHJ-11; j: SHJ-19; k, n-o: HL 234.
All photographs are at the same scale; white scale bar (e) = 500 µm.

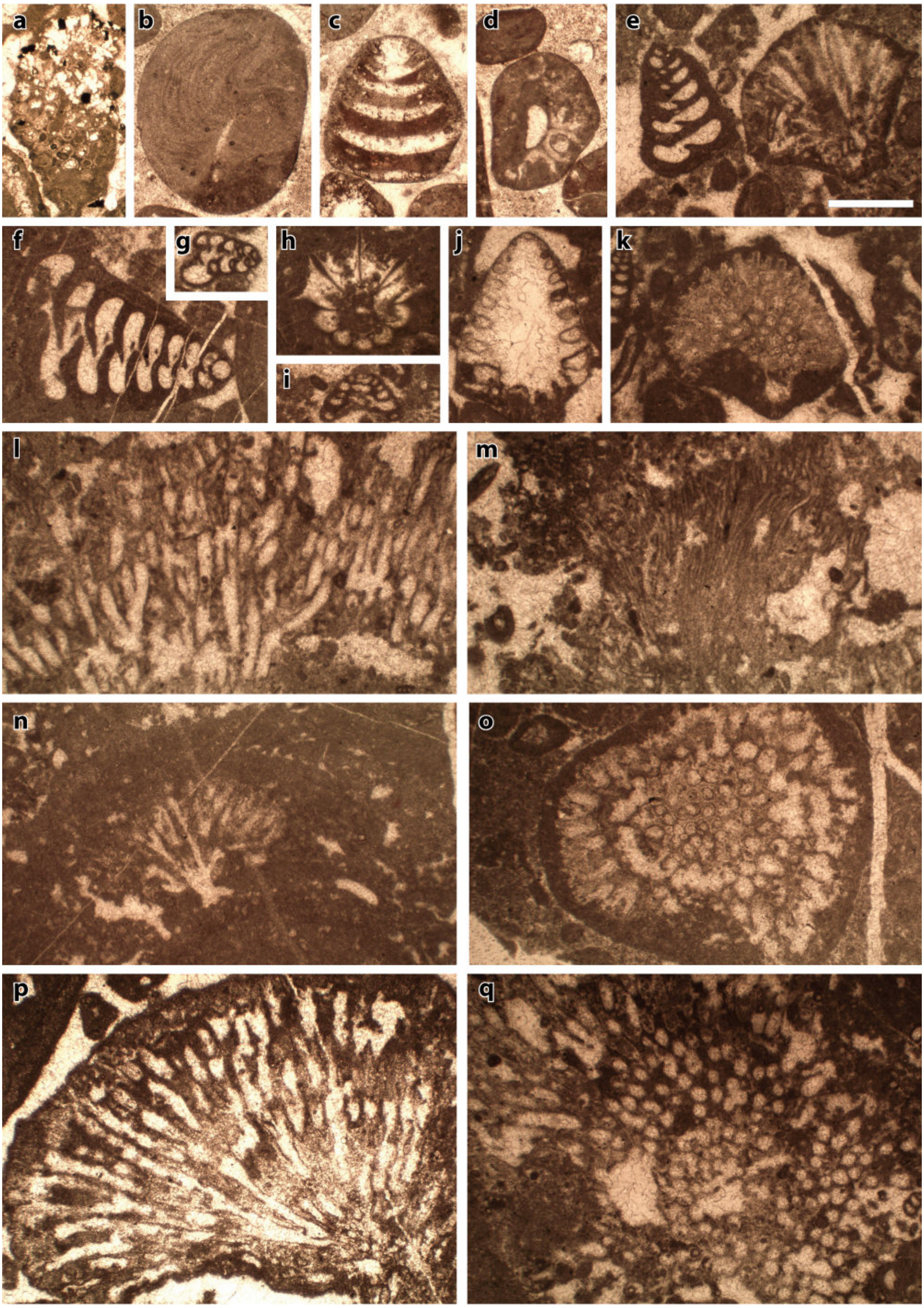
a
b
c
d
e
f
g
h
i
j
k
l
m
n
o
p
q

Plate 2: Morro de Sant Jordi, **figs. a-c:** fenestrae, interpreted as evidence of gas bubbles, most likely methane, trapped within a fine-grained peloidal matrix (SHJ-1); **figs. d-f:** endolithic ostracods occurring in open fractures (d) or intergranular pores (e-f); **fig. g:** coprolites; **figs. h-i:** burrows developed within sedimentary sills (pink dotted lines) and fractures (black dotted lines); **fig. j:** calcarenite extraclast from Unit 2 reworked into sedimentary sills; **fig. k:** calcarenite extraclast from Unit 2 reworked into Unit 6 as the nucleus of a ferruginous oncoid; **fig. l:** wackestone extraclast with *Aloisalthella* from Unit 1 reworked into Unit 6 as the nucleus of a ferruginous oncoid.
All images (a-i) were obtained by transmitted-light optical microscopy. a-c: SHJ-1; d: SHJ-3B; e-g: HL 234; h-i: HL 235; j: SHJ-3bis; k-l: SHJ-12.
All photographs, except h-i, are at the same scale: white scale bar (in a) = 500 μm; black scale bar = 1 cm (h-i).

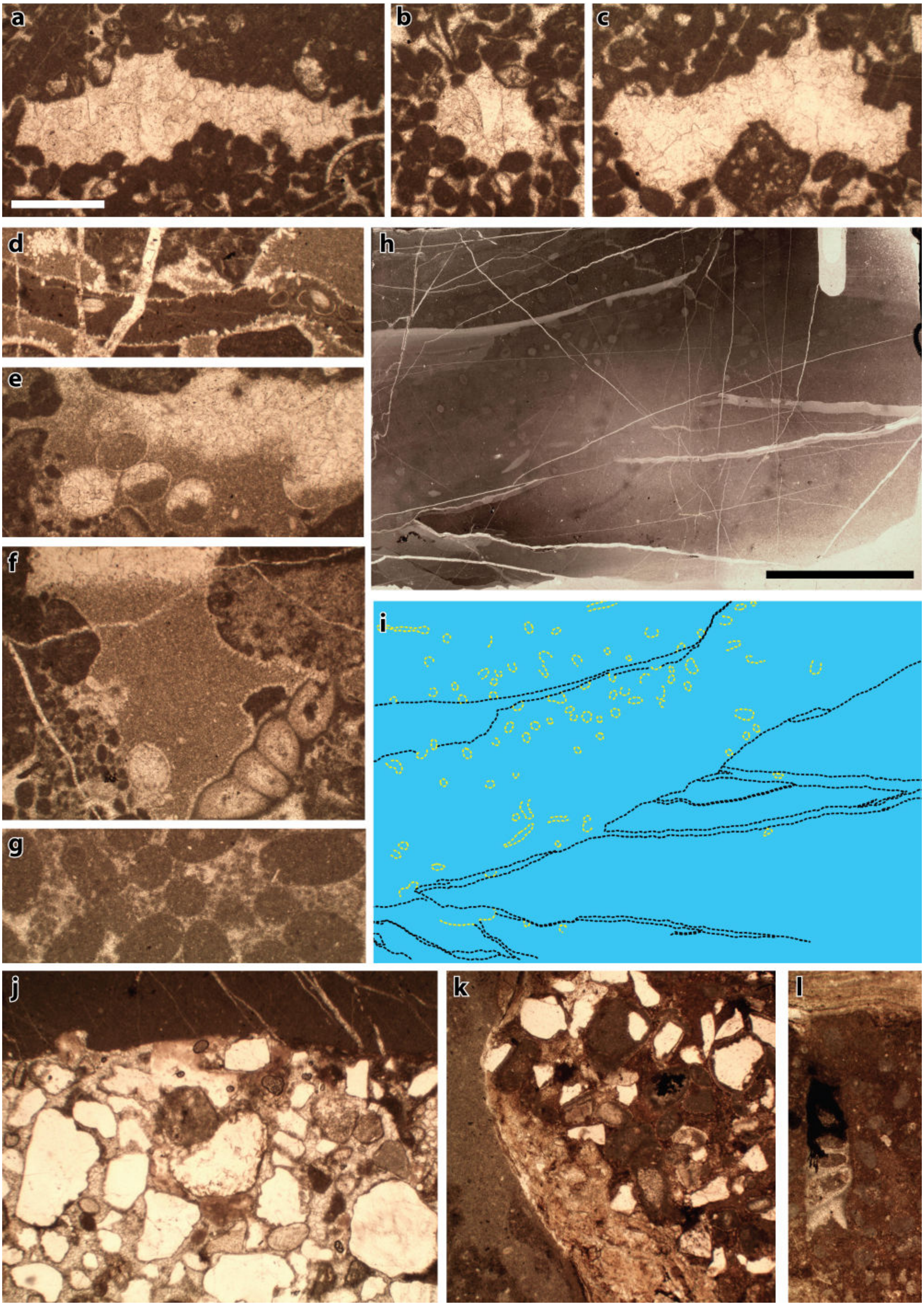
a
b
c
d
e
f
g
h
i
j
k
l

Plate 3: figs. a-b: General views of Punta de la Pila, with the flat abrasion surface (indicated by orange arrows) at the top right of the images and the YÉBENES cave (the white arrow points to a black cobble also visible in c-d); **fig. c:** The YÉBENES cave, with a tentative outline of its sedimentary infill (marked by a dotted blue line); **fig. d:** Close-up view of the sedimentary infill; **figs. e-g:** Views from the unconformity surface of the chimneys that fed the karstic network; at their intersection with the surface, the chimneys may appear either as an elongated slot (e), oriented N70°E (WSW-ENE), or as narrow, irregular openings, either connected (f) or isolated (g). White scale bars = 1 m (c-d); black scale bars = 10 cm (e-g).


a
b
c
d
e
f
g

Plate 4: figs. a-c: The discontinuity at Punta de la Pila (white dotted lines) is a slight angular unconformity consisting of a flat abrasion surface with borings (a, b left), passing rightward into an irregular surface that ends in a pronounced step (b right, c); **fig. d:** Another pronounced step is observed at the level of the present-day cobble beach, together with a modern notch at sea level; **fig. e:** cluster of *Leviathania sautieri* (COQUAND, 1856); **figs. f-g:** sedimentary infills in the YÉBENES paleocave; **fig. h:** clavate borings (*e.g.*, *Gastrochaenolites*) filled by the overlying crust on the upper surface of the Jurassic limestones.


a
b
c
d
e
f
g
h

Plate 5: figs. a-f, g *pars*, h-k: *Salpingoporella annulata* (CAROZZI, 1953); **figs. g *pars*, t, v, w *pars*, x:** *Aloisalthella sulcata* (ALTH, 1882); **fig. l:** diagenetic sequence with cement 1, fracture 1 (Φ1), sedimentary infill 1 (si1), fracture 2 (Φ2), cement 2, fracture 3 (Φ3), sedimentary infill 2 (si2) [SHJ-2]; **fig. m:** *Mohlerina basiliensis* (MOHLER, 1938); **fig. n:** *Pseudocyclammina lituus* (YOKOYAMA, 1890); **fig. o:** diagenetic sequence with cement 1, sedimentary infill 1 (si1), fracture 2 (Φ2), cement 2, fracture 3 (Φ3), sedimentary infill 2 (si2) with endolithic ostracods, no evidence of fracture 1 (Φ1) as in l [SHJ-3B]; **fig. p:** diagenetic sequence with cement 1, sedimentary infill 1 (si1), late cement (hc2) [SHJ-3H]; **fig. q:** diagenetic sequence with micritisation, leaching in the meteoric vadose zone, cement 1 (early hc1), sedimentary infill 1 (si1), cement 2 (late hc1), breakage of the micritic envelop, sedimentary infill 2 (si2), late cement (hc2) [SHJ-3B]; **figs. r-s:** diagenetic sequence with cement 1 (hc1), colored calcite band, sedimentary infill 1 (si1), late cement (hc2) [SHJ-2]; **fig. u:** diagenetic sequence with cement 1 (hc1), sedimentary infill 1 (si1), late cement (hc2) [SHJ-3B]; **fig. y:** cement 1 (hc1), sedimentary infill 1 (si1), cement 2 (hc2), fracture (Φ), sedimentary infill 2 (si2) [SHJ-3H]; **fig. w *pars*:** *Redmondoides lugeoni* (SEPTFONTAINE, 1977).
Caption: hc, hyaline calcite; si, sedimentary infill; Φ, fracture wall.
All images (a-y) are in optical microscopy transmitted light. a: SHJ-1bis; b, d-e, h, j-k: SHJ-11; c, g, w: HL 234; f, v: SHJ-3Mi; i: HL 238; l, o, q, t-u: SHJ-3B; m, r-s: SHJ-2; n: HL 231; p, x-y: SHJ-3H.
All photomicrographs are shown at the same scale; black scale bar = 250 µm.

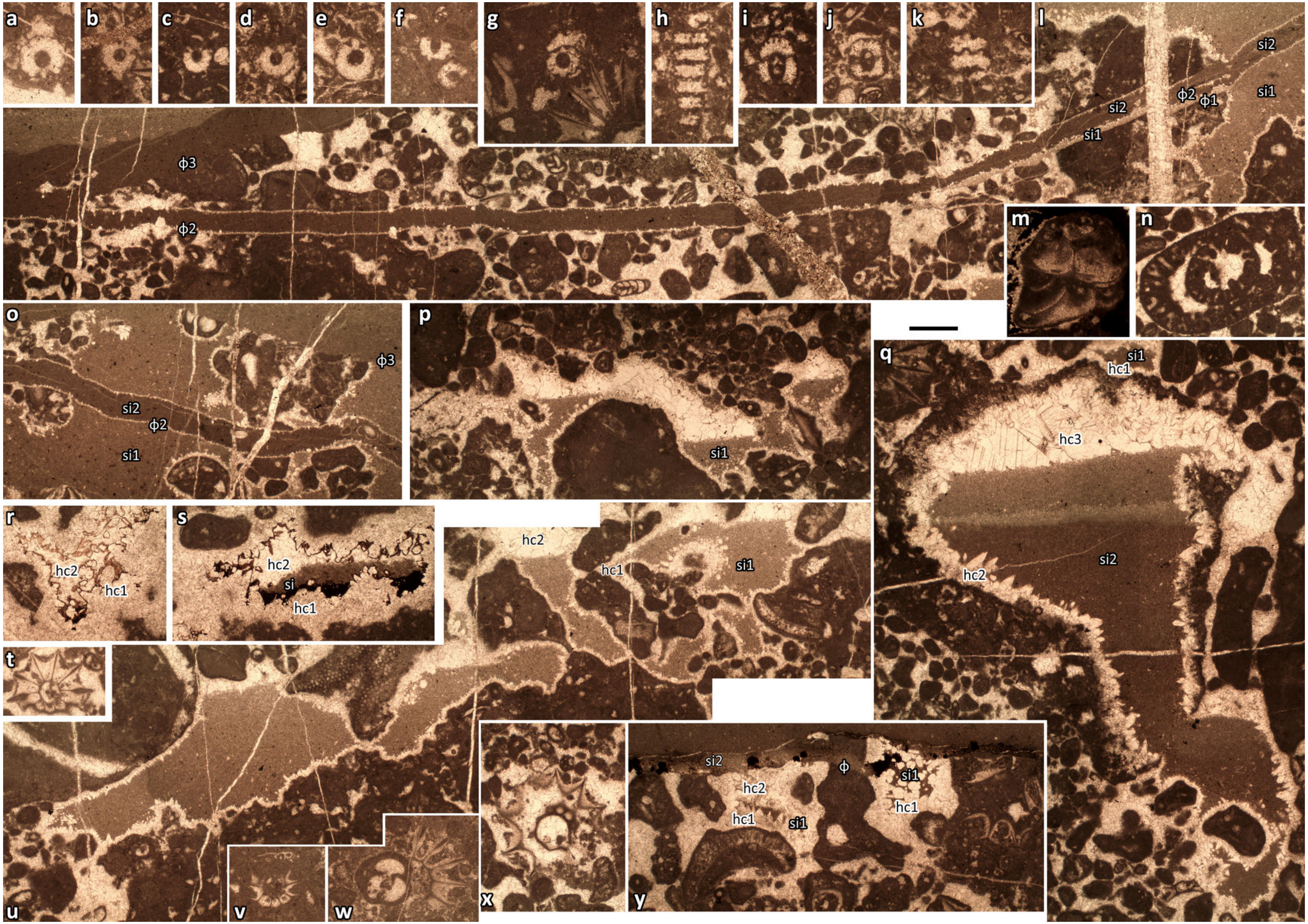
a
b
c
d
e
f
g
h
i
j
k
l
si2
si1
ϕ2
ϕ1
si2
si1
ϕ3
ϕ2
m
n
o
ϕ3
si2
ϕ2
si1
p
si1
q
si1
hc1
hc3
si2
hc2
r
hc2
hc1
s
hc2
si
hc1
hc2
hc1
si1
t
u
v
w
x
y
si2
hc2
ϕ
si1
hc1
si1
hc1

Plate 6: Diagenetic sequence in sample SHJ-19, description in the text, **figs. a-b:** cathodoluminescence exposure time 10 seconds (08/04/2026); **fig. c:** cathodoluminescence exposure time 5 seconds (27/03/2026). Diagenetic sequence in sample SHJ-3bis, **figs. d-e:** dark band within the crystal zonation; **figs. f-g:** dark fringe around the allochems, most likely of endostromatolitic origin; **fig. h:** pitted appearance of the cloudy sparite, reflecting the presence of impurities within the crystals.
Caption: es, endostromatolites; cc, cloudy calcite; hc, hyaline calcite; the yellow band marks the boundary between hc1 and hc2.
Images a-c: optical cathodoluminescence microscopy; images d-h: scanning electron microscopy (e-h: BSE-COMP, back scattering electron and composition; i-l: UVD, ultra variable-pressure detector).
Optical cathodoluminescence microscopy: all photomicrographs are shown at the same scale; white scale bars = 250 µm (a-c); scanning electron microscopy: scales = 200 µm (h), 500 µm (d-e), 1 mm (f-g).

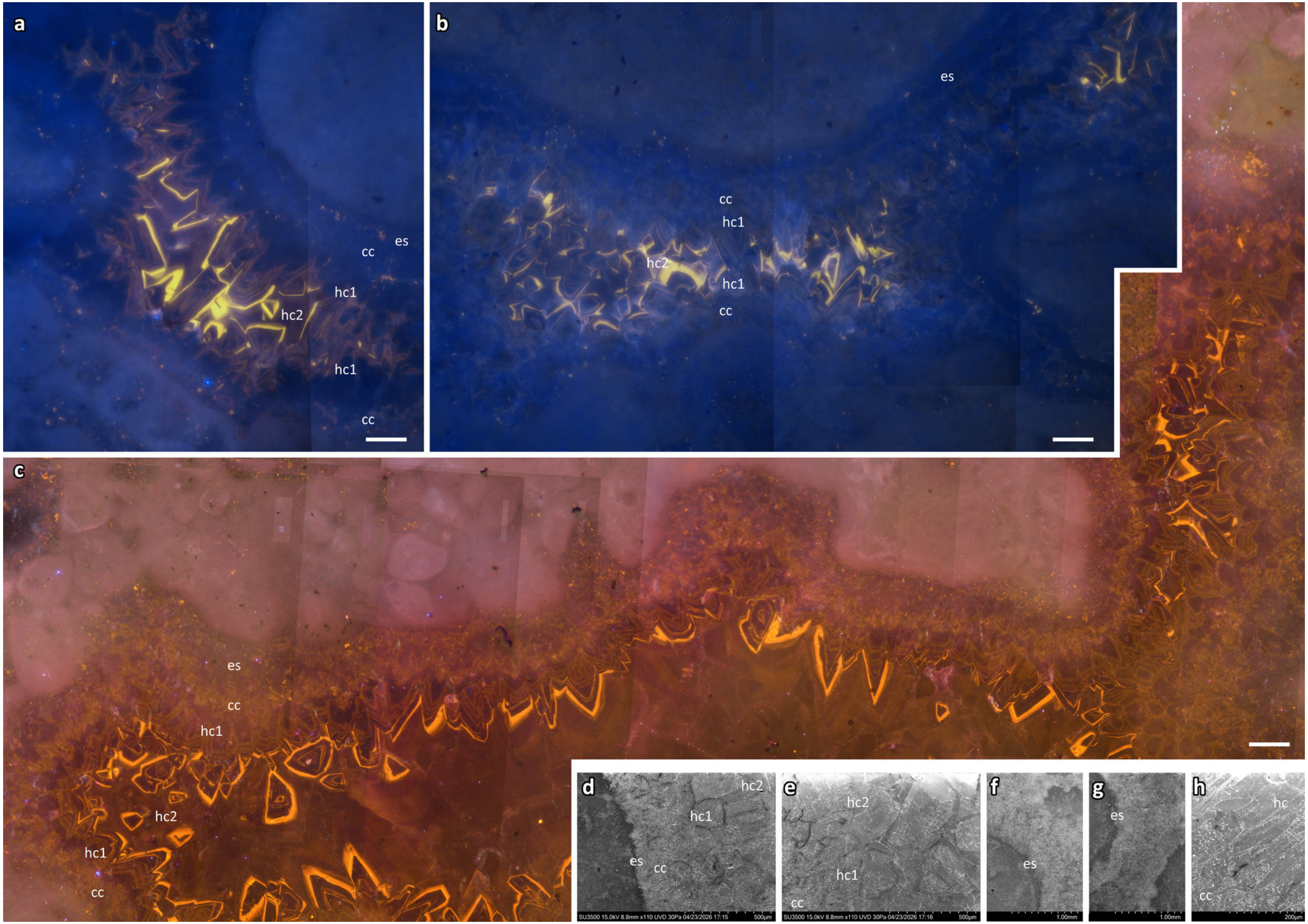
a
cc
es
hc1
hc2
hc1
cc
b
es
cc
hc1
hc2
hc1
cc
c
es
cc
hc1
hc2
hc1
cc
d
hc2
hc1
es
cc
e
hc2
hc1
cc
f
es
g
es
h
hc
cc

Plate 7: Diagenetic sequence in sample SHJ-19, description in the text, **figs. a-c:** exposure time 10 seconds (08/04/2026); **fig. d:** exposure time 5 seconds (27/03/2026). Diagenetic sequence in sample SHJ-3bis, **fig. e:** dissolution zoning of some crystals on the polished, then slightly etched surface; **figs. f-h:** BSE-COMP images illustrating competitive growth of blade-like calcite crystals, which become progressively larger toward the center of the pore, characteristic of drusy cementation. Note that the proximal parts of the blades are cloudy, whereas the distal parts are homogeneous; **figs. i-l:** UVD images illustrating the drusic cement.
Caption: es, endostromatolites; cc, cloudy calcite; hc, hyaline calcite; the yellow (or orange) band marks the boundary between hc1 and hc2; si, geopetal micritic sedimentary infill; Φ, fracture.
Images a-d: optical cathodoluminescence microscopy; images e-l: scanning electron microscopy (e-h: BSE-COMP, back scattering electron and composition; i-l: UVD, ultra variable-pressure detector).
Optical cathodoluminescence microscopy: white scale bars = 250 µm (a, c); yellow scale bars = 500 µm (b, d); scanning electron microscopy: scales = 50 µm (e), 300 µm (j-l), 400 µm (f-i).

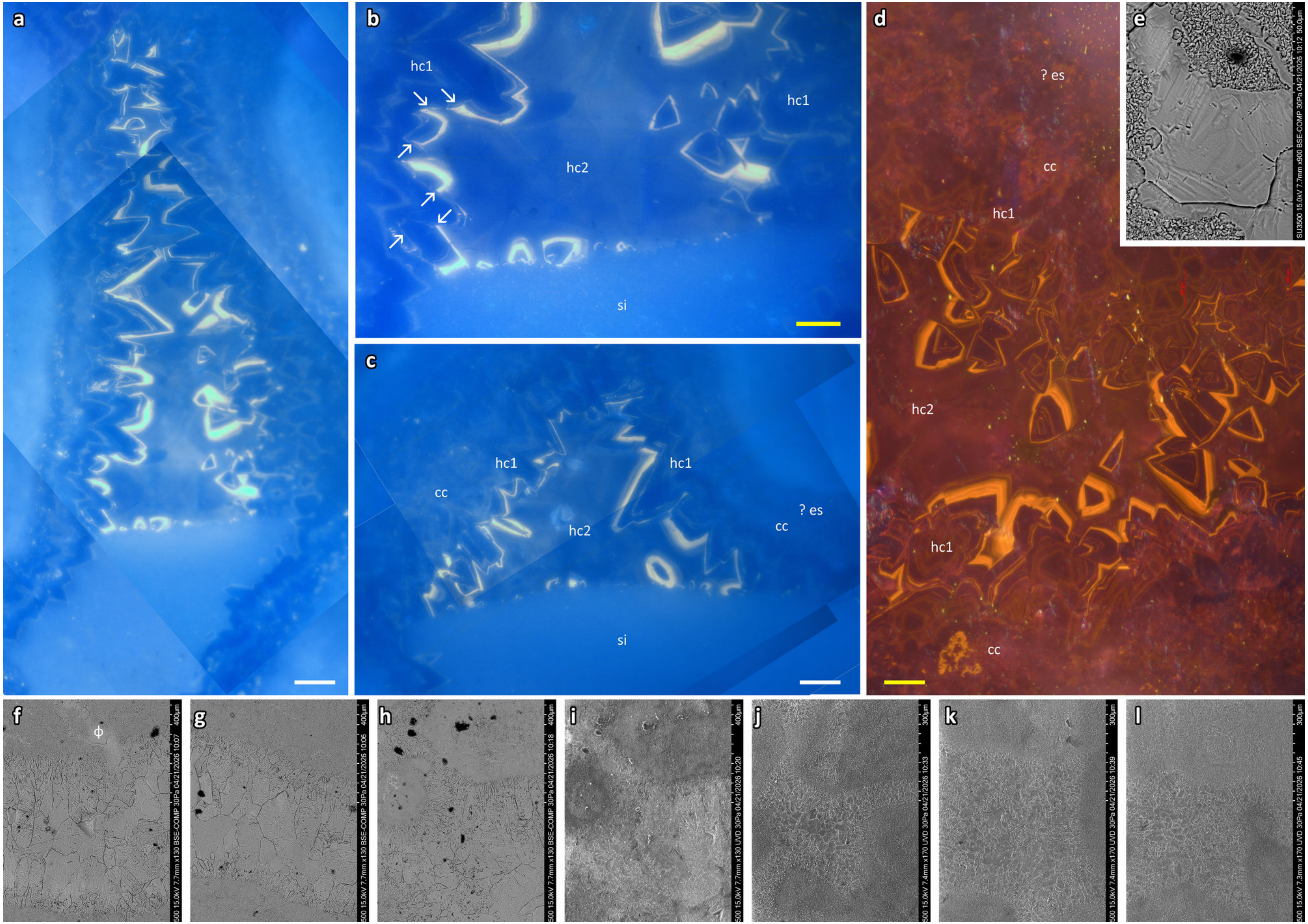
a
b
hc1
hc1
hc2
si
c
hc1
hc1
cc
hc2
? es
cc
si
d
? es
cc
hc1
hc2
hc1
cc
e
f
g
h
i
j
k
l